J. Fluid Mech. (2001), *vol.* 436, *pp.* 283–320. Printed in the United Kingdom

The dynamics of a laminar flow in a symmetric channel with a sudden expansion

By T. HAWA[1] AND Z. RUSAK[2]

[1]Institute for Mathematics and its Applications, University of Minnesota, Minneapolis, MN 55455, USA

[2]Department of Mechanical Engineering, Aeronautical Engineering and Mechanics, Rensselaer Polytechnic Institute, Troy, NY 12180-3590, USA

(Received 10 August 1998 and in revised form 18 November 2000)

Bifurcation analysis, linear stability study, and direct numerical simulations of the dynamics of a two-dimensional, incompressible, and laminar flow in a symmetric long channel with a sudden expansion with right angles and with an expansion ratio D/d (d is the width of the channel inlet section and D is the width of the outlet section) are presented. The bifurcation analysis of the steady flow equations concentrates on the flow states around a critical Reynolds number $Re_c(D/d)$ where asymmetric states appear in addition to the basic symmetric states when $Re \geqslant Re_c(D/d)$. The bifurcation of asymmetric states at Re_c has a pitchfork nature and the asymmetric perturbation grows like $\sqrt{Re - Re_c(D/d)}$. The stability analysis is based on the linearized equations of motion for the evolution of infinitesimal two-dimensional disturbances imposed on the steady symmetric as well as asymmetric states. A neutrally stable asymmetric mode of disturbance exists at $Re_c(D/d)$ for both the symmetric and the asymmetric equilibrium states. Using asymptotic methods, it is demonstrated that when $Re < Re_c(D/d)$ the symmetric states have an asymptotically stable mode of disturbance. However, when $Re > Re_c(D/d)$, the symmetric states are unstable to this mode of asymmetric disturbance. It is also shown that when $Re > Re_c(D/d)$ the asymmetric states have an asymptotically stable mode of disturbance. The direct numerical simulations are guided by the theoretical approach. In order to improve the numerical simulations, a matching with the asymptotic solution of Moffatt (1964) in the regions around the expansion corners is also included. The dynamics of both small- and large-amplitude disturbances in the flow is described and the transition from symmetric to asymmetric states is demonstrated. The simulations clarify the relationship between the linear stability results and the time-asymptotic behaviour of the flow. The current analyses provide a theoretical foundation for previous experimental and numerical results and shed more light on the transition from symmetric to asymmetric states of a viscous flow in an expanding channel. It is an evolution from a symmetric state, which loses its stability when the Reynolds number of the incoming flow is above $Re_c(D/d)$, to a stable asymmetric equilibrium state. The loss of stability is a result of the interaction between the effects of viscous dissipation, the downstream convection of perturbations by the base symmetric flow, and the upstream convection induced by two-dimensional asymmetric disturbances.

1. Introduction

Laminar two-dimensional flow in a symmetric channel with a sudden expansion exhibits a transition phenomenon from symmetric to asymmetric equilibrium states

as the Reynolds number of the flow, Re, is increased. The experimental studies of Durst, Melling & Whitelaw (1974), Cherdron, Durst & Whitelaw (1978), Sobey & Drazin (1986), Fearn, Mullin & Cliffe (1990), and Durst, Pereira & Tropea (1993) demonstrated for channels with moderate expansion ratios that when Re is relatively low the flow in the channel is steady, two-dimensional, and symmetric with two separation zones near the expansion corners, the size of which increases with Re. However, at higher values of Re, the flow stays two-dimensional and steady but becomes asymmetric with two separation zones of different lengths which attach on either the upper or the lower wall of the channel. At even higher Re, additional recirculation zones appear along the channel walls.

The numerical and experimental studies of Fearn *et al.* (1990) show that asymmetric steady flow states can be numerically simulated and the observed transition behaviour may occur as a bifurcation of asymmetric states from the symmetric states at a certain critical Re_c. They demonstrated that it may be a pitchfork symmetry-breaking bifurcation point where the symmetric state loses its stability and evolves into the asymmetric state when $Re > Re_c$. Shapira, Degani & Weihs (1990) conducted linear stability studies that are based on an energy functional. They numerically solved the stability equations for certain channel expansion ratios and various angles of expansion. They also found the change of stability at Re_c.

Recently, Battaglia *et al.* (1997) have conducted numerical linear stability studies as well as steady flow simulations to investigate the effect of the channel expansion ratio on the appearance of the asymmetric states. They used concepts of bifurcation theory to numerically determine the bifurcation point. They found that the critical Reynolds number at which the transition to asymmetric states occurs decreases with increasing channel expansion ratio. Also, Alleborn *et al.* (1997) have used numerical continuation methods and numerical linear stability studies to clarify the effect of a slight asymmetry in the channel geometry on the flow behaviour. They also extended the steady-state bifurcation diagrams to higher values of Re, found higher-order bifurcation points, and demonstrated the effects of these on the steady-state solutions.

Drikakis (1997) investigated the influence of various discretization schemes, from second order up to fourth order of numerical accuracy, and numerical solvers on the simulations of the steady-state bifurcation phenomenon in a sudden expansion channel flow. He found that the third- and fourth-order finite difference schemes are needed to compute values of Re_c which are very close to those found in the stability studies of Shapira *et al.* (1990). He also showed that Re_c decreases with the increase of the expansion ratio of the channel and that the asymmetry increases with Re.

Soong, Tzeng & Hsieh (1998) conducted numerical studies of laminar, plane, twin-jet flows injected into a channel with sudden expansions. Time-dependent computations were performed in the search for unsteady or asymmetric flow states. They found steady asymmetric flow patterns as well as flow instabilities and associated bifurcation phenomena which are related to the jet Reynolds number, sidewall confinement, and the jet proximity. Specifically, an unexpected Hopf bifurcation phenomenon of unsteady periodic states was revealed in these two-dimensional flow cases.

The review of the previous experimental and numerical studies on the topic shows that the transition from symmetric to asymmetric states in a viscous flow in an expanding channel may be related to the bifurcation of steady-state solutions of the Navier–Stokes equations at Re_c and to the change of stability across this point. Yet, most of the previous studies concentrated on either the numerical computations of the steady states or on the linear stability investigations of the symmetric states. The relationship between the previous bifurcation/linear stability analyses and the

direct numerical simulations using the unsteady Navier–Stokes equations was not constructed in detail and is not obvious. Also, the experimental and numerical investigations describe the change in the flow characteristics but do not provide a clear physical mechanism for the change of stability at the critical Re. A comprehensive theoretical and computational approach which clarifies the above issues is of great interest and may shed more light on the flow physics.

The objective of this paper is to present an analysis of the evolution of two-dimensional viscous flows in a channel with a sudden expansion, to clarify the relationship between the static bifurcation of solutions of the steady Navier–Stokes equations and the change of stability related to the bifurcation point, to provide more insight into the relationship between the linear stability results and unsteady flow simulations, and to identify the mechanism by which asymmetric states appear in the flow dynamics. To achieve these goals, asymptotic and stability analyses around the critical Reynolds number are proper as well as necessary, in order to carefully explore the balance between the viscous and convection effects on the dynamics of perturbations. The theoretical approach also provides a framework in which direct numerical simulations of the transition process in laminar flows in an expanding channel are conducted.

The paper presents bifurcation analysis, linear stability study, and numerical simulations of a laminar flow in a symmetric channel with a sudden expansion with right angles. The outline of the paper is as follows. The mathematical problem is defined in § 2. The bifurcation analysis (§ 3) focuses on the flow states around Re_c where steady asymmetric states may appear in addition to the basic symmetric states when $Re \geqslant Re_c$. The stability analysis (§ 4) shows that a neutral asymmetric mode of disturbance exists at the critical state for both the symmetric and the asymmetric equilibrium states. It is demonstrated that the symmetric states change their stability characteristics as the Reynolds number changes around the critical level. When $Re < Re_c$ an asymptotically stable mode is found, and when $Re > Re_c$ an unstable mode of disturbance may evolve. It is also shown that when $Re > Re_c$, the asymmetric states have an asymptotically stable mode of disturbance. Guided by the theoretical approach, direct numerical simulations based on the unsteady Navier–Stokes equations are conducted (§ 5). In order to improve the numerical simulations, a matching with the asymptotic solution of Moffatt (1964) in the regions around the expansion corners are also included (see the Appendix). The simulations describe the evolution of both small- and large-amplitude disturbances in the flow (§ 6). The transition from symmetric to asymmetric states is demonstrated. The simulations clarify the relationship between the linear stability results and the evolution of the flow. They also show that the unstable mode according to the linear theory dominates the flow dynamics at Re around Re_c. The paper is concluded (§ 7) with a possible physical mechanism which governs the flow transition.

It should also be mentioned here that the recent works of Rusak & Hawa (1999) and Hawa & Rusak (2000) provide an additional insight into the two-dimensional flow dynamics in an expanding channel. Rusak & Hawa (1999) focused on a weakly nonlinear analysis of the flow dynamics which explores the special nonlinear interactions between the unsteady, convective, and viscous effects. The analysis resulted in an ordinary, nonlinear, first-order differential equation (similar to the Landau equation) which may describe the evolution of the amplitude of a special eigenmode of perturbation as function of Re near Re_c. The analytical solution showed that when $Re < Re_c$ the symmetric state is stable. However, when $Re \geqslant Re_c$ the symmetric state loses its stability and evolves into the asymmetric state, as also found in the present

paper. The flow evolution, as described by the nonlinear model, showed agreement with time-history plots from direct numerical simulations using the unsteady Navier–Stokes equations. Hawa & Rusak (2000) extended the work of Rusak & Hawa (1999) by including the nonlinear effect of a slight asymmetry in the channel geometry on the flow evolution. It was found that channel asymmetry changes the pitchfork bifurcation diagram of a flow in a symmetric channel into two separate branches of equilibrium states. The primary branch describes a gradual and stable change of the flow states from symmetric to asymmetric as Re is increased across Re_c. The secondary branch appears at a certain modified critical Reynolds number, $Re_{c\tau} > Re_c$, and describes two additional asymmetric flow states for each $Re > Re_{c\tau}$ which are disconnected from the primary branch. The large-amplitude asymmetric states along the secondary branch are stable whereas the small-amplitude states are unstable. Again, the asymptotic results demonstrated agreement with numerical simulations and experimental data for Re near Re_c.

2. Mathematical model

The flow of a two-dimensional, viscous, Newtonian, and incompressible fluid is studied in a long channel of width d, which suddenly expands symmetrically, with right angles, to a long channel of width D where $D > d$ (see figure 1). Axial and transverse lengths, $\bar{x}$ and $\bar{y}$, are scaled by the upstream channel width d, $x = \bar{x}/d$ and $y = \bar{y}/d$. The flow field is described in a Cartesian coordinate system (x, y), where $y = 0$ is the centreline of the channel, and $x = 0$ is the expansion section of the channel. The inlet section to the channel is located at $x = -x_0$ (where $x_0 \gg 1$) and tends to $-\infty$. The outlet section of the channel is located at $x = x_1$ (where $x_1 \gg 1$) and tends to $+\infty$. Along the upstream section of the channel, $x < 0$, the lower wall is at $y = -1/2$ and the upper wall is at $y = 1/2$. At $x = 0$, the lower wall is given along the segment $-D/2d \leqslant y \leqslant -1/2$ and the upper wall along the segment $1/2 \leqslant y \leqslant D/2d$. Along the channel section where $x > 0$, the lower wall is at $y = -D/2d$ and the upper wall is at $y = D/2d$. We define the flow domain inside the expanding channel as A. All velocities are normalized by U_{ave}, the averaged velocity of the Poiseuille flow far upstream of the channel expansion at the inlet section. The time $\bar{t}$ is scaled by d/U_{ave}, $t = \bar{t}U_{ave}/d$. The Reynolds number characterizing the flow problem is defined as

$$Re = \frac{U_{ave}d}{\nu} \tag{1}$$

where ν is the kinematic viscosity. The non-dimensional Navier–Stokes equations in the vorticity–stream function formulation are given by (Batchelor 1967)

$$\Omega_t + u\Omega_x + v\Omega_y = \frac{1}{Re}\left(\Omega_{xx} + \Omega_{yy}\right), \tag{2}$$

$$\Omega = -(\psi_{xx} + \psi_{yy}), \tag{3}$$

$$u = \psi_y, \quad v = -\psi_x. \tag{4}$$

Here $\Omega(x, y, t)$ denotes the vorticity, $\psi(x, y, t)$ denotes the stream function, and $u(x, y, t)$, $v(x, y, t)$ are the axial and transverse velocity components, respectively. Equation (2) is the vorticity transport equation of motion, and (3) is the Poisson equation relating the stream function and the vorticity. The relations (4) show that the stream function, ψ, identically satisfies the two-dimensional continuity equation for an incompressible flow, $u_x + v_y = 0$. The use of the vorticity–stream function formulation reduces the

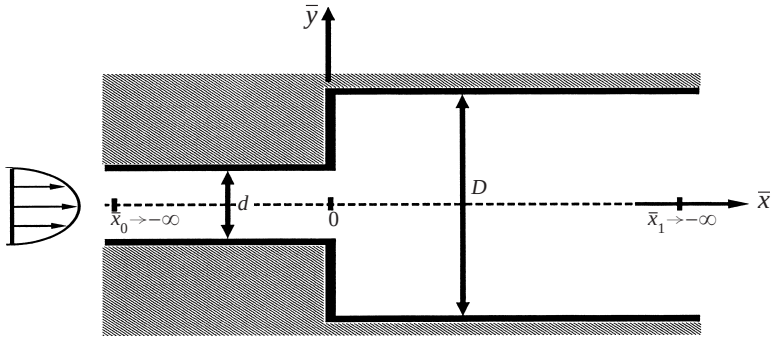

FIGURE 1. Sketch of a two-dimensional channel with a symmetric sudden expansion.

flow equations to a single fourth-order partial differential equation for the evolution of the stream function. It also eliminates the pressure from the equations and, thereby, simplifies the boundary conditions needed for a solution of the problem. These equations are used to solve the dynamics of the entire flow field except at the expansion corners where the vorticity is singular.

The boundary conditions along the lower and upper walls are the tangency and no-slip conditions, i.e. for all time t

$$u = 0, \quad v = 0, \quad \psi = \begin{cases} -1/2 & \text{along the lower wall,} \\ 1/2 & \text{along the upper wall.} \end{cases} \tag{5}$$

A steady Poiseuille flow velocity profile is considered at the inlet section ($x = -x_0$), i.e. for all time t and for $-1/2 \leqslant y \leqslant 1/2$:

$$v(x = -x_0 \to -\infty, y, t) = 0, \tag{6}$$

$$u(x = -x_0 \to -\infty, y, t) = \tfrac{3}{2}(1 - 4y^2), \tag{7}$$

$$\psi(x = -x_0 \to -\infty, y, t) = \tfrac{3}{2}(y - \tfrac{4}{3}y^3), \tag{8}$$

$$\Omega(x = -x_0 \to -\infty, y, t) = 12y. \tag{9}$$

Outlet flow far downstream of the channel is also assumed to have a fully developed (steady and columnar) velocity profile, i.e. for all time t and $-D/2d \leqslant y \leqslant D/2d$

$$\psi_x(x = x_1 \to \infty, y, t) = 0, \quad \Omega_x(x = x_1 \to \infty, y, t) = 0. \tag{10}$$

The conditions (5)–(10) were used in all of the numerical studies of the problem (Fearn *et al.* 1990; Battaglia *et al.* 1997; Drikakis 1997; and Alleborn *et al.* 1997). They may reflect the physical situation as reported in the experiments of Durst *et al.* (1974, 1993) and Fearn *et al.* (1990).

The problem defined by equations (1)–(10) is well posed and describes the evolution of the flow in a channel for every Re and D/d. We consider here some relevant initial conditions for the stream function and the vorticity, such as a perturbed symmetric state in the channel at $t = 0$

$$\psi(x, y, 0) = \psi_s(x, y; Re; D/d) + \epsilon_\psi(x, y), \quad \Omega(x, y, 0) = \Omega_s(x, y; Re; D/d) + \epsilon_\Omega(x, y). \tag{11}$$

Here, the symmetric-state solution, $\psi_s(x, y; Re; D/d)$ and $\Omega_s(x, y; Re; D/d) = -(\psi_{s_{xx}} + \psi_{s_{yy}})$, is obtained numerically by solving the steady-state version of the problem (1)–(10) in half of the domain, where $y > 0$, and imposing the symmetry conditions,

$v = 0, u_y = 0$, along the x-axis. This numerical solution is based on an iterative procedure and is used later in §§ 3.1 and 3.2 to compute symmetric states. The solution ψ_s, and the related Ω_s, for the entire domain is found by reflecting the flow in the upper region to the lower region. This method of constructing the symmetric state is specifically needed when $Re > Re_c$ where asymmetries dominate the flow dynamics (1)–(10) in the full domain.

In (11), $\epsilon_\psi(x, y)$ and $\epsilon_\Omega(x, y)$ are prescribed disturbances. These disturbances may have small or large amplitudes. The objective of the paper is to study the evolution of the disturbances.

In order to understand the dynamics of the flow in the channel as described by (1)–(11), it is important to identify the steady-state solutions of the system (1)–(10). Some of these solutions may be symmetric about the x-axis and others asymmetric states. Also, some of the equilibrium states may be stable and others unstable to two-dimensional perturbations. In the following sections we define the critical Reynolds number, Re_c, explore the nature of the steady-state solutions of (1)–(10) around Re_c, and investigate their stability characteristics.

3. Bifurcation analysis

3.1. *Asymptotic analysis of symmetric states*

Using symmetry considerations about the x-axis, steady symmetric solutions $\psi_s(x, y; Re; D/d)$ of equations (1)–(10) can be constructed for every Reynolds number Re and expansion ratio D/d. We look for a critical Reynolds number Re_c where, for a fixed ratio D/d, steady asymmetric states suddenly bifurcate from the branch of the symmetric states. To obtain such a critical (bifurcation) state, the stream function ψ_s and the vorticity Ω_s are expanded in the neighbourhood of Re_c in the following standard manner:

$$\psi_s = \psi_s^* + \frac{\Delta Re}{Re_c}\psi_1\left(x, y, \frac{D}{d}\right) + \cdots, \tag{12}$$

$$\Omega_s = \Omega_s^* + \frac{\Delta Re}{Re_c}\Omega_1\left(x, y, \frac{D}{d}\right) + \cdots. \tag{13}$$

Here ψ_s^* and Ω_s^* are the steady-state symmetric solutions of (1)–(4) at Re_c and they satisfy the boundary conditions (5)–(10). Also, in (12) and (13), $\Delta Re = Re - Re_c$ and $|\Delta Re|/Re_c \ll 1$. As Re tends to Re_c, the term $1/Re$ can be expanded as

$$\frac{1}{Re} = \frac{1}{Re_c + \Delta Re} = \frac{1}{Re_c}\left(1 - \frac{\Delta Re}{Re_c} + \cdots\right). \tag{14}$$

Inserting the above expansions, (12)–(14), into the steady-state version of the vorticity–stream function equations (2)–(4) results at the leading order $O(\Delta Re/Re_c)$ in a linearized system of the steady-state equations of motion

$$\Omega_{s\,x}^*\psi_{1y} + \psi_{s\,y}^*\Omega_{1x} - \Omega_{s\,y}^*\psi_{1x} - \psi_{s\,x}^*\Omega_{1y} - \frac{1}{Re_c}(\Omega_{1xx} + \Omega_{1yy}) = \frac{-1}{Re_c}(\Omega_{s\,xx}^* + \Omega_{s\,yy}^*), \tag{15}$$

$$\Omega_1 = -(\psi_{1xx} + \psi_{1yy}). \tag{16}$$

Notice that (15) is a non-homogeneous linear partial differential equation. The boundary conditions for the velocity and stream function are specified by using (5)–(10). Since the leading terms ψ_s^* and Ω_s^* satisfy those conditions, the perturbation term

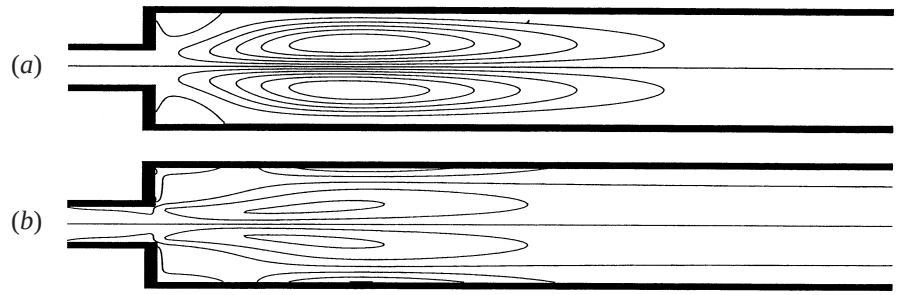

FIGURE 2. The functions (*a*) ψ_1 and (*b*) Ω_1 for the case where $D/d = 3$.

ψ_1 and velocity perturbations $u_1 = \psi_{1y}$ and $v_1 = -\psi_{1x}$ must satisfy homogeneous boundary conditions

$$u_1 = v_1 = \psi_1 = 0 \tag{17}$$

at the channel inlet and along the upper and lower walls. The vorticity perturbation also has to satisfy $\Omega_1 = 0$ at the inlet. At the channel outlet, the perturbations must satisfy

$$\psi_{1x} = \Omega_{1x} = 0. \tag{18}$$

Equations (15)–(18) formulate a linear non-homogeneous problem for the calculation of the perturbation function ψ_1 for any Re_c and expansion ratio D/d. It can be shown that the solution of ψ_1 describes a symmetric flow perturbation about the x-axis which actually presents the change of the symmetric state ψ_s from ψ_s^* as Re slightly deviates from Re_c. Therefore, the problem given by (15)–(18) does not provide a critical state of bifurcation. Yet, as we can see later, the solution of this problem is essential in the study of the stability of the symmetric states.

The problem (15)–(18) can be solved numerically using standard finite-difference methods. However, in the present paper, we use an alternative method to compute ψ_1 and Ω_1 which is based on the numerical solution of the steady-state version of (1)–(10). Using the iterative procedure of solution in half of the domain, two steady and symmetric flow states at Reynolds numbers Re_a and Re_b around the critical value Re_c (yet to be determined) can be computed. We use the following estimation:

$$\left.\begin{aligned} \psi_1 &= \frac{\psi_s(x, y; Re_b; D/d) - \psi_s(x, y; Re_a; D/d)}{Re_b - Re_a} Re_c, \\ \Omega_1 &= \frac{\Omega_s(x, y; Re_b; D/d) - \Omega_s(x, y; Re_a; D/d)}{Re_b - Re_a} Re_c. \end{aligned}\right\} \tag{19}$$

This computation is a numerical finite-difference approximation of ψ_1 and Ω_1 which helps to avoid the solution of (15)–(18). An example of streamline and vorticity contours of the functions ψ_1 and Ω_1, respectively, for the case $D/d = 3$ where $Re_c = 53.8$ (for details of determining the critical Reynolds number Re_c see § 3.2) is presented in figure 2. These functions were computed based on the steady-state symmetric solutions at $Re_a = 51.0$ and $Re_b = 54.0$. It is clear that ψ_1 creates a symmetric perturbation to the symmetric flow.

3.2. *Critical state for bifurcation of asymmetric states*

To obtain the critical state for the bifurcation of steady asymmetric flows, the stream function and vorticity for steady asymmetric flow at Re close to Re_c are now expanded

in a different approach:

$$\psi_{as}(x, y; Re; \tfrac{D}{d}) = \psi_s^* + \epsilon_\alpha \psi_\alpha + \epsilon_\beta \psi_\beta + \epsilon_\gamma \psi_\gamma + \cdots, \tag{20}$$

$$\Omega_{as}(x, y; Re; \tfrac{D}{d}) = \Omega_s^* + \epsilon_\alpha \Omega_\alpha + \epsilon_\beta \Omega_\beta + \epsilon_\gamma \Omega_\gamma + \cdots, \tag{21}$$

where $0 < \epsilon_\gamma \ll \epsilon_\beta \ll \epsilon_\alpha \ll 1$. Subscripts α, β, and γ denote the first-, second-, and third-order perturbations to the base critical state. It is expected from previous numerical and experimental studies that near the critical state the flow leading-order perturbations to the symmetric base flow are much greater than the flow changes in the symmetric states described by (12), (13), and (19). Therefore, it is assumed that $\epsilon_\alpha \gg |\Delta Re|/Re_c$.

Inserting the above expansions (20), (21), and (14) into the steady version of the vorticity-transport equations (2)–(4), results in the leading-order terms $O(\epsilon_\alpha)$ in a linearized homogeneous system of the steady-state equations of motion,

$$\Omega_{s\,x}^* \psi_{\alpha y} + \psi_{s\,y}^* \Omega_{\alpha x} - \Omega_{s\,y}^* \psi_{\alpha x} - \psi_{s\,x}^* \Omega_{\alpha y} - \frac{1}{Re_c}(\Omega_{\alpha xx} + \Omega_{\alpha yy}) = 0, \tag{22}$$

$$\Omega_\alpha = -(\psi_{\alpha xx} + \psi_{\alpha yy}). \tag{23}$$

The analysis of the next-order equations, $O(\epsilon_\beta)$ and $O(\epsilon_\gamma)$, shows

$$\epsilon_\beta \left(\Omega_{s\,x}^* \psi_{\beta y} + \psi_{s\,y}^* \Omega_{\beta x} - \Omega_{s\,y}^* \psi_{\beta x} - \psi_{s\,x}^* \Omega_{\beta y} - \frac{1}{Re_c}(\Omega_{\beta xx} + \Omega_{\beta yy}) \right)$$
$$+\epsilon_\alpha^2(\psi_{\alpha y}\Omega_{\alpha x} - \psi_{\alpha x}\Omega_{\alpha y}) + \frac{\Delta Re}{Re_c}\frac{1}{Re_c}(\Omega_{s\,xx}^* + \Omega_{s\,yy}^*) = 0, \tag{24}$$

$$\Omega_\beta = -(\psi_{\beta xx} + \psi_{\beta yy}), \tag{25}$$

and

$$\epsilon_\gamma \left(\Omega_{s\,x}^* \psi_{\gamma y} + \psi_{s\,y}^* \Omega_{\gamma x} - \Omega_{s\,y}^* \psi_{\gamma x} - \psi_{s\,x}^* \Omega_{\gamma y} - \frac{1}{Re_c}(\Omega_{\gamma xx} + \Omega_{\gamma yy}) \right)$$
$$+\epsilon_\alpha\epsilon_\beta(\psi_{\alpha y}\Omega_{\beta x} + \psi_{\beta y}\Omega_{\alpha x} - \psi_{\alpha x}\Omega_{\beta y} - \psi_{\beta x}\Omega_{\alpha y}) + \epsilon_\alpha \frac{\Delta Re}{Re_c}\frac{1}{Re_c}(\Omega_{\alpha xx} + \Omega_{\alpha yy}) = 0, \tag{26}$$

$$\Omega_\gamma = -(\psi_{\gamma xx} + \psi_{\gamma yy}). \tag{27}$$

The boundary conditions (5)–(10) result in homogeneous conditions for ψ_α, $u_\alpha = \psi_{\alpha y}$, $v_\alpha = -\psi_{\alpha x}$ and Ω_α:

$$u_\alpha = v_\alpha = \psi_\alpha = 0 \tag{28}$$

at the channel inlet and along the upper and lower walls. Also, $\Omega_\alpha = 0$ at the inlet. At the channel outlet we have

$$\psi_{\alpha x} = \Omega_{\alpha x} = 0. \tag{29}$$

Similar conditions apply to ψ_β, Ω_β and $\psi_\gamma, \Omega_\gamma$.

The problem described by (22)–(23) with boundary conditions (28)–(29) formulates an eigenvalue problem for the solution of the critical Reynolds number Re_c and the corresponding eigenfunction ψ_α. Notice that this is a very complicated problem since the eigenvalue Re_c appears not only as a free parameter but also inside the formulation of the base flow functions ψ_s^* and Ω_s^*. This problem was numerically solved by using either a restarted, iterative Arnoldi method as described in Alleborn *et al.* (1997) or the Cayley transform techniques coupled with subspace iterations used by Battaglia *et al.* (1997). These numerical solutions demonstrated the possible existence of a

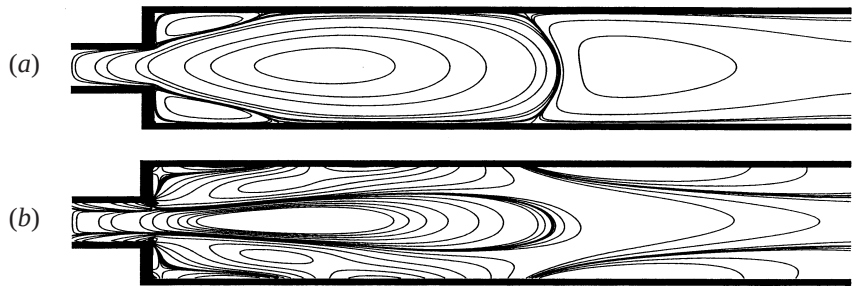

FIGURE 3. The functions (*a*) ψ_α and (*b*) Ω_α for the case where $D/d = 3$.

finite, first, positive eigenvalue which is defined as the critical Reynolds number Re_c. Also, note that this problem may have more eigenvalues, greater than Re_c, but those are beyond the interest of the present paper (see, for example, Alleborn *et al.* 1997 who found higher-order eigenvalues). It is clear that Re_c is a function of the ratio D/d. Examples of such calculations are given in Alleborn *et al.* (1997) and Battaglia *et al.* (1997). It was also found that the eigenfunction ψ_α is a real function and describes an asymmetric perturbation to the base symmetric flow at Re_c. Therefore, it can be postulated from the previous numerical studies that the solution of (22)–(23) with boundary conditions (28)–(29) provides the critical state for the bifurcation of asymmetric states and the structure of these states in the neighbourhood of Re_c.

In the present paper we compute Re_c, the eigenfunction ψ_α, and the related vorticity Ω_α using an alternative approach. The critical Reynolds number is found from the dynamical simulations of (1)–(11) described later in § 6. From the computed flow evolution at a given Re and D/d, we calculate the decay or growth rate of the perturbations to the symmetric state. Re_c is defined as the lowest Reynolds number where the decay rate vanishes (where the growth rate of the perturbations to the symmetric state changes its sign from negative to positive). The solution of the eigenfunction is approximated by the following formulae:

$$\left.\begin{aligned} k_0\psi_\alpha &= \frac{\psi_{as}(x,y;\widetilde{Re};D/d) - \psi_s(x,y;\widetilde{Re};D/d)}{(\widetilde{Re}-Re_c)^{1/2}}Re_c^{1/2}, \\ k_0\Omega_\alpha &= \frac{\Omega_{as}(x,y;\widetilde{Re};D/d) - \Omega_s(x,y;\widetilde{Re};D/d)}{(\widetilde{Re}-Re_c)^{1/2}}Re_c^{1/2}. \end{aligned}\right\} \tag{30}$$

Here the Reynolds number $\widetilde{Re}$ is close to the critical value Re_c and satisfies $0 < (\widetilde{Re} - Re_c)/Re_c \ll 1$. The symmetric solution at $\widetilde{Re}$, ψ_s and Ω_s, is computed by the numerical iterative procedure of the steady-state problem of (1)–(10) in half of the domain where $y > 0$ and with symmetry conditions along the centreline. The asymmetric state at $\widetilde{Re}$, ψ_{as} and Ω_{as}, is numerically determined from the time-asymptotic solution of the flow dynamics according to (1)–(11). The constant k_0 in (30) is determined from the following higher-order analysis.

An example of streamline and vorticity contours of the functions ψ_α and Ω_α, respectively, for the case $D/d = 3$ where $Re_c = 53.8$ (determined from the computations of the flow dynamics in § 6) is presented in figure 3. These functions were computed based on the steady-state symmetric and asymmetric solutions at $\widetilde{Re} = 54.0$. Figure 3 shows that ψ_α creates an asymmetric perturbation to the symmetric flow. The value of Re_c and shape of ψ_α and Ω_α presented here are very similar to those reported by Battaglia *et al.* (1997) for the case $D/d = 3$.

The second-order problem described by (24)–(25) and boundary conditions similar to (28)–(29) suggests that for the richest case $\epsilon_\beta = \Delta Re/Re_c$ and $\epsilon_\alpha^2 = k_0^2 \Delta Re/Re_c$. We also find that the solution for $\epsilon_\beta \psi_\beta$ is given by

$$\epsilon_\beta \psi_\beta = \frac{\Delta Re}{Re_c}(\psi_1 + k_0^2 \psi_{1\alpha}) \tag{31}$$

where ψ_1 is the solution of the problem given by (15)–(18), and $\psi_{1\alpha}$ is the solution of the problem

$$\epsilon_\beta \left(\Omega^*_{s\,x}\psi_{1\alpha y} + \psi^*_{s\,y}\Omega_{1\alpha x} - \Omega^*_{s\,y}\psi_{1\alpha x} - \psi^*_{s\,x}\Omega_{1\alpha y} - \frac{1}{Re_c}(\Omega_{1\alpha xx} + \Omega_{1\alpha yy}) \right) = -k_0^2 \frac{\Delta Re}{Re_c}(\psi_{\alpha y}\Omega_{\alpha x} - \psi_{\alpha x}\Omega_{\alpha y}), \tag{32}$$

$$\Omega_{1\alpha} = -(\psi_{1\alpha xx} + \psi_{1\alpha yy}), \tag{33}$$

with boundary conditions for $\psi_{1\alpha}$ similar to (28)–(29). The problem for $\psi_{1\alpha}$ can be solved numerically using standard finite-difference methods. Notice, however, that the coefficient k_0 cannot be determined from a solvability condition of (32)–(33) since multiplying (32) by ψ_α, integrating over the flow domain A, and using the boundary conditions (28) and (29) gives

$$\iint_A (\psi_{\alpha y}\Omega_{\alpha x} - \psi_{\alpha x}\Omega_{\alpha y})\psi_\alpha \, \mathrm{d}y \, \mathrm{d}x = 0. \tag{34}$$

In the present work, the functions $\psi_{1\alpha}$ and $\Omega_{1\alpha}$ are numerically approximated using the estimations

$$k_0^2 \frac{\Delta Re}{Re_c}\psi_{1\alpha}(x, y; D/d) \sim \psi_{as}(x, y; Re; D/d) - \psi_s(x, y; Re; D/d) - \sqrt{\frac{\Delta Re}{Re_c}} k_0 \psi_\alpha(x, y; D/d)$$

and

$$k_0^2 \frac{\Delta Re}{Re_c}\Omega_{1\alpha}(x, y; D/d) \sim \Omega_{as}(x, y; Re; D/d) - \Omega_s(x, y; Re; D/d) - \sqrt{\frac{\Delta Re}{Re_c}} k_0 \Omega_\alpha(x, y; D/d)$$

for Re near Re_c. For example, when $D/d = 3$ we compute $\psi_{1\alpha}$ from the steady symmetric and asymmetric solutions at $Re = 58.0$. These functions are described in figure 4. It can be seen that the second-order perturbation function $\psi_{1\alpha}$ creates an asymmetric flow disturbance in the expansion channel as a direct effect of the eigenfunction ψ_α.

To determine k_0 we may use the third-order problem given by (26)–(27). Using the solution (31) for $\epsilon_\beta \psi_\beta$ we find

$$\epsilon_\gamma \left(\Omega^*_{s\,x}\psi_{\gamma y} + \psi^*_{s\,y}\Omega_{\gamma x} - \Omega^*_{s\,y}\psi_{\gamma x} - \psi^*_{s\,x}\Omega_{\gamma y} - \frac{1}{Re_c}(\Omega_{\gamma xx} + \Omega_{\gamma yy}) \right) + k_0 \left(\frac{\Delta Re}{Re_c} \right)^{3/2} \left(\psi_{\alpha y}\Omega_{1x} + \psi_{1y}\Omega_{\alpha x} - \psi_{\alpha x}\Omega_{1y} - \psi_{1x}\Omega_{\alpha y} + \frac{1}{Re_c}(\Omega_{\alpha xx} + \Omega_{\alpha yy}) \right) + k_0^3 \left(\frac{\Delta Re}{Re_c} \right)^{3/2} (\psi_{\alpha y}\Omega_{1\alpha x} + \psi_{1\alpha y}\Omega_{\alpha x} - \psi_{\alpha x}\Omega_{1\alpha y} - \psi_{1\alpha x}\Omega_{\alpha y}) = 0. \tag{35}$$

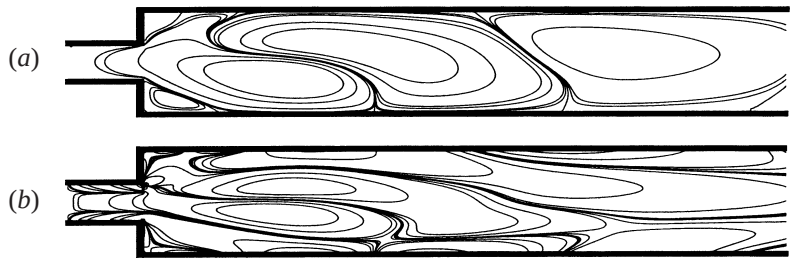

FIGURE 4. The functions (*a*) $\psi_{1\alpha}$ and (*b*) $\Omega_{1\alpha}$ for the case where $D/d = 3$.

Assuming $|\epsilon_\gamma| \ll (\Delta Re/Re_c)^{3/2}$, multiplying (35) by ψ_α, and integrating over the flow domain A gives

$$k_0 = \pm\left[\frac{-\iint_A \left(\psi_{\alpha y}\Omega_{1x} + \psi_{1y}\Omega_{\alpha x} - \psi_{\alpha x}\Omega_{1y} - \psi_{1x}\Omega_{\alpha y} + \frac{1}{Re_c}(\Omega_{\alpha xx} + \Omega_{\alpha yy})\right)\psi_\alpha \,\mathrm{d}y\,\mathrm{d}x}{\iint_A (\psi_{\alpha y}\Omega_{1\alpha x} + \psi_{1\alpha y}\Omega_{\alpha x} - \psi_{\alpha x}\Omega_{1\alpha y} - \psi_{1\alpha x}\Omega_{\alpha y})\psi_\alpha \,\mathrm{d}y\,\mathrm{d}x}\right]^{1/2}. \tag{36}$$

The numerical estimations of ψ_1, Ω_1, ψ_α, Ω_α, $\psi_{1\alpha}$, and $\Omega_{1\alpha}$, provide the information needed to compute k_0. The calculation of the term in the brackets in (36) shows that it is positive for $D/d = 3$, k_0 has two opposite real values, and the bifurcation at Re_c is pitchfork bifurcation. We also found similar results for the case $D/d = 2$. From the work of Battaglia *et al.* (1997) it may be concluded that this result is correct for other values of D/d in the range $2 \leqslant D/d \leqslant 12$.

The above asymptotic analysis demonstrates that the solution of the leading order term exists only when $Re > Re_c$. Therefore, when $Re > Re_c$, steady asymmetric states, $\psi_{as}(x, y; Re; D/d) = \psi_s^*(x, y; Re_c; D/d) + (\Delta Re/Re_c)^{1/2} k_0 \psi_\alpha(x, y; D/d) + \cdots$, exist in addition to the basic steady symmetric states, $\psi_s(x, y; Re; D/d) = \psi_s^*(x, y; Re_c; D/d) + (\Delta Re/Re_c)\psi_1(x, y; D/d) + \cdots$. However, when $Re < Re_c$, only the symmetric states exist. These arguments clarify the nature of the critical state at Re_c as a bifurcation point for the steady asymmetric states. Equation (36) reflects that the bifurcation is a result of the nonlinear interaction between the perturbations ψ_1, ψ_α and $\psi_{1\alpha}$. The $\pm$ sign in (36) shows that the asymmetric states may be established in two possible ways which are anti-symmetric to each other. The bifurcation of asymmetric states has a pitchfork nature, i.e. the asymmetric perturbation to the symmetric state can exist only when $\Delta Re > 0$ and it grows near the critical Reynolds number like $(\Delta Re/Re_c)^{1/2}$. This result is in good agreement with the bifurcation diagrams obtained from the numerical studies of Alleborn *et al.* (1997), Drikakis (1997), and Battaglia *et al.* (1997).

4. Stability analysis

In this section we study the stability of the symmetric and asymmetric steady states described in § 3.

4.1. *Stability analysis of symmetric states around Re_c*

To consider the stability of the symmetric states $\psi_s(x, y; Re; D/d)$ we let

$$\psi = \psi_s + \epsilon\tilde{\psi}(x, y, t) + \cdots, \tag{37}$$

$$\Omega = \Omega_s + \epsilon\tilde{\Omega}(x, y, t) + \cdots, \tag{38}$$

where $0 < \epsilon \ll |\Delta Re|/Re_c$, $\tilde{\psi}$ is an unsteady stream function disturbance, and $\tilde{\Omega}$ is an unsteady vorticity disturbance. We look for the evolution of the disturbances in the channel as described by equations (1)–(4) and boundary conditions (5)–(10). Substituting (37)–(38) into the unsteady vorticity-transport equations (2)–(4) and neglecting second order terms, we obtain to the leading order $O(\epsilon)$ the linearized equations of motion,

$$\tilde{\Omega}_t + \psi_{s_y}\tilde{\Omega}_x + \Omega_{s_x}\tilde{\psi}_y - \psi_{s_x}\tilde{\Omega}_y - \Omega_{s_y}\tilde{\psi}_x - \frac{1}{Re}(\tilde{\Omega}_{xx} + \tilde{\Omega}_{yy}) = 0, \tag{39}$$

$$\tilde{\Omega} = -(\tilde{\psi}_{xx} + \tilde{\psi}_{yy}).$$

The boundary conditions for $\tilde{\psi}$ and $\tilde{\Omega}$ are similar to (28)–(29) for all time t.

In studying the linearized stability problem we consider a suitable mode analysis of (39) of the form

$$\tilde{\psi}(x, y, t) = \mathrm{e}^{\sigma t}\tilde{\phi}(x, y), \tag{40}$$

$$\tilde{\Omega}(x, y, t) = \mathrm{e}^{\sigma t}\tilde{\Phi}(x, y), \tag{41}$$

where, in the general case, the perturbation growth rate σ may be a complex number and $\tilde{\phi}$ and $\tilde{\Phi}$ are complex functions. Substituting these expressions into (39) we obtain an eigenvalue system for solving σ, $\tilde{\phi}$, and $\tilde{\Phi}$:

$$\sigma\tilde{\Phi} + \Omega_{s_x}\tilde{\phi}_y + \psi_{s_y}\tilde{\Phi}_x - \Omega_{s_y}\tilde{\phi}_x - \psi_{s_x}\tilde{\Phi}_y - \frac{1}{Re}(\tilde{\Phi}_{xx} + \tilde{\Phi}_{yy}) = 0, \tag{42}$$

$$\tilde{\Phi} = -(\tilde{\phi}_{xx} + \tilde{\phi}_{yy}). \tag{43}$$

The boundary conditions (5)–(10) result in homogeneous conditions for $\tilde{\phi}$, $\tilde{u} = \tilde{\phi}_y$, $\tilde{v} = -\tilde{\phi}_x$, and $\tilde{\Phi}$:

$$\tilde{u} = \tilde{v} = \tilde{\phi} = 0 \tag{44}$$

at the channel inlet and along the upper and lower walls. Also, $\tilde{\Phi} = 0$ at the inlet. At the channel outlet we have

$$\tilde{\phi}_x = \tilde{\Phi}_x = 0. \tag{45}$$

The problem (42)–(45) is an eigenvalue problem for solving the general relationship between the perturbation growth rate and Reynolds number, $\sigma(Re)$. The solution of this problem presents a challenge and is complicated to achieve even by using numerical methods (see, for example, Alleborn *et al.* 1997). However, it is important to observe from (42)–(45) that when $\sigma = 0$ a neutrally stable mode of disturbance exists when

$$\Omega_{s_x}\tilde{\phi}_y + \psi_{s_y}\tilde{\Phi}_x - \Omega_{s_y}\tilde{\phi}_x - \psi_{s_x}\tilde{\Phi}_y - \frac{1}{Re}(\tilde{\Phi}_{xx} + \tilde{\Phi}_{yy}) = 0, \tag{46}$$

$$\tilde{\Phi} = -(\tilde{\phi}_{xx} + \tilde{\phi}_{yy}), \tag{47}$$

with boundary conditions (44)–(45). The eigenvalue problem defined by (46)–(47) with conditions (44)–(45) has a solution only at the eigenvalue Reynolds numbers described by the problem (22)–(23) and (28)–(29), specifically when $Re = Re_c$ (the first eigenvalue). This shows the interesting relationship, at $Re = Re_c$: $\sigma = 0$, $\tilde{\phi} \equiv \psi_\alpha$, and $\tilde{\Phi} \equiv \Omega_\alpha$. This means that the critical symmetric state ψ_s^* at Re_c is also, from a dynamical perspective, a neutrally stable state with respect to the eigenmode at Re_c.

We show now that the critical state at Re_c is also a point of exchange of stability for the branch of symmetric states in the channel. We concentrate on the neighbourhood of Re_c and use the following asymptotic analysis. Using the results from the previous paragraph, it is expected that as Re approaches Re_c also $\sigma = \sigma_R + \mathrm{i}\sigma_I$ tends to zero, i.e. both the real part σ_R and the imaginary part σ_I tend to zero. Also, when Re approaches Re_c the symmetric states ψ_s, and the related Ω_s, are described by the asymptotic expansions (12) and (13). Therefore, we consider the asymptotic expansions for $\tilde{\phi}$ and $\tilde{\Phi}$ in the limit as $Re \to Re_c$ (or $\sigma \to 0$) in the form

$$\tilde{\phi} = \psi_\alpha + \epsilon_1 \tilde{\phi}_R + \mathrm{i}\epsilon_2 \tilde{\phi}_I + \cdots, \tag{48}$$

$$\tilde{\Phi} = \Omega_\alpha + \epsilon_1 \tilde{\Phi}_R + \mathrm{i}\epsilon_2 \tilde{\Phi}_I + \cdots, \tag{49}$$

where ϵ_1 and ϵ_2 are small parameters which depend on Re and tend to 0 as Re tends to Re_c.

Substituting (48)–(49) into (42)–(43) and using (12)–(14) results in two equations from the real and imaginary parts of (42)–(43) for the solution of $\tilde{\phi}_R$ and $\tilde{\phi}_I$:

the real part is

$$\begin{aligned}\sigma_R \Omega_\alpha + \frac{\Delta Re}{Re_c}\left[\psi_{\alpha y}\Omega_{1x} + \Omega_{\alpha x}\psi_{1y} - \psi_{\alpha x}\Omega_{1y} - \Omega_{\alpha y}\psi_{1x} + \frac{1}{Re_c}(\Omega_{\alpha xx} + \Omega_{\alpha yy})\right] \\ + \epsilon_1\left[\Omega^*_{s\,x}\tilde{\phi}_{Ry} + \psi^*_{s\,y}\tilde{\Phi}_{Ry} - \Omega^*_{s\,y}\tilde{\phi}_{Rx} - \psi^*_{s\,x}\tilde{\Phi}_{Ry} - \frac{1}{Re_c}(\tilde{\Phi}_{Rxx} + \tilde{\Phi}_{Ryy})\right] \\ - \sigma_I\epsilon_2\tilde{\Phi}_I + O\left(\epsilon_1\sigma_R, \epsilon_1\frac{\Delta Re}{Re_c}\right) = 0,\end{aligned} \tag{50}$$

$$\tilde{\Phi}_R = -(\tilde{\phi}_{Rxx} + \tilde{\phi}_{Ryy}), \tag{51}$$

and the imaginary part is

$$\begin{aligned}\sigma_I\Omega_\alpha + \sigma_R\epsilon_2\tilde{\Phi}_I + \epsilon_2\left[\Omega^*_{s\,x}\tilde{\phi}_{Iy} + \psi^*_{s\,y}\tilde{\Phi}_{Ix} - \Omega^*_{s\,y}\tilde{\phi}_{Ix} - \psi^*_{s\,x}\tilde{\Phi}_{Iy} - \frac{1}{Re_c}(\tilde{\Phi}_{Ixx} + \tilde{\Phi}_{Iyy})\right] \\ + O\left(\epsilon_1\sigma_I, \epsilon_2\frac{\Delta Re}{Re_c}\right) = 0,\end{aligned} \tag{52}$$

$$\tilde{\Phi}_I = -\left(\tilde{\phi}_{Ixx} + \tilde{\phi}_{Iyy}\right). \tag{53}$$

The asymptotic relations (52) and (53) show that $\sigma_I = O(\epsilon_2)$. Actually, the numerical studies of Alleborn *et al.* (1997) demonstrated that around Re_c the imaginary part vanishes, $\sigma_I = 0$. Therefore, in the asymptotic relations (50) and (51) the term with $\sigma_I\epsilon_2$ may be neglected. Also, from these relations it may be concluded that $\sigma_R = O(\Delta Re/Re_c)$. Therefore,

$$\sigma_R = k_s\frac{\Delta Re}{Re_c} \tag{54}$$

where k_s is a constant to be determined. The dynamical simulations in §6 can be used to estimate the sign and value of k_s. It is found that the stability rate parameter of the symmetric states $k_s > 0$. For example, the numerical study in §6 shows that $Re_c = 53.8$ and $k_s = 0.105 \pm 0.002$ when $D/d = 3$. The numerical studies of Alleborn *et al.* (1997) and Battaglia *et al.* (1997) indicate that $k_s > 0$ for a wider range of expansion ratios $2 \leqslant D/d \leqslant 12$.

To compute the stability coefficient k_s, we propose that $|\epsilon_1| \ll \Delta Re/Re_c$. Therefore, multiplying (50) by ψ_α and integrating over the flow domain A gives

$$k_s = \frac{-\iint_A \left(\psi_{\alpha_y}\Omega_{1x} + \psi_{1_y}\Omega_{\alpha x} - \psi_{\alpha_x}\Omega_{1y} - \psi_{1_x}\Omega_{\alpha y} + \frac{1}{Re_c}(\Omega_{\alpha xx} + \Omega_{\alpha yy}) \right) \psi_\alpha \, dy \, dx}{\iint_A (\psi_{\alpha x}^2 + \psi_{\alpha y}^2) \, dy \, dx}. \tag{55}$$

Here the relation

$$\iint_A \Omega_\alpha \psi_\alpha \, dy \, dx = \iint_A (\psi_{\alpha x}^2 + \psi_{\alpha y}^2) \, dy \, dx$$

has been used. The numerical estimations of ψ_1, Ω_1, ψ_α, and Ω_α provide the information needed to compute k_s. For example, when $D/d = 3$ and using ψ_1 and ψ_α as shown in figures 2 and 3, we find $k_s = 0.102$ which is in good agreement with the value for $k_s = 0.105$ which was obtained out of the unsteady simulations. This may also justify the assumption that $|\epsilon_1| \ll |\Delta Re|/Re_c$ made above.

The results (54) and (55) show that as Re is increased across the critical Reynolds number Re_c the real part of the growth rate σ of the perturbation mode (40) and (41) changes from negative to positive. This proves that the critical state at Re_c is a point of exchange of stability for the steady symmetric solutions of (1)–(10), i.e. the symmetric states in the channel lose their stability as Re is increased toward Re_c and are unstable to a certain mode of perturbation, which is essentially the eigenfunction ψ_α, for every $Re > Re_c$. Equations (54) and (55) reflect that the change of stability of the symmetric states is a result of the nonlinear interaction between the flow perturbations ψ_1 and ψ_α.

Equations (39)–(41), (48), and (49) can now be used to explain the mechanism by which the symmetric states lose their stability. It can be seen from (39) that three major effects compete one with the other on the stability of the base symmetric flow. These are: (i) the convection of the vorticity perturbation by the axial velocity of the base flow, (ii) the convection of the base flow vorticity by the axial flow perturbations, and (iii) the viscous dissipation of the vorticity perturbation. Effect (i) tends to convect the perturbations downstream and has a stabilizing influence. Effect (ii) is related to the shape of the perturbation. Equations (40), (41), (48), and (49) show that the most important perturbation is the one which is related to the eigenmode ψ_α. This perturbation creates an upstream axial speed on one side of the channel and a downstream axial speed on the other side of the channel. Therefore, it has a destabilizing effect specifically on the side of the channel where upstream speed is induced. The viscous dissipation (iii) has also a stabilizing effect. The combination of these effects determines the stability of the base symmetric flow. When Re is relatively small, the viscous dissipation is large and dominant and the flow is stable. As Re is increased, the viscous dissipation effect decreases like $1/Re$ and, therefore, the symmetric flow becomes less stable. At Re_c there is a critical balance between the destabilizing upstream convection effects of the asymmetric perturbation and the combined stabilizing effects of the viscous dissipation and the downstream convection by the base flow. When Re is further increased, the upstream convection effects of the asymmetric perturbation become dominant and, therefore, the symmetric flow becomes unstable. The larger Re is, the more unstable the symmetric flow becomes. Also, the larger D/d is, the smaller the effect of convection of the vorticity perturbation by the axial velocity of the base flow, and, therefore, the lower Re_c is.

4.2. *Stability analysis of asymmetric states bifurcating at Re_c*

To consider the stability of the asymmetric states $\psi_{as}(x, y; Re; D/d)$ given by (20)–(21), (30)–(31), and (36) when $Re \geqslant Re_c$

$$\left.\begin{aligned}\psi_{as}(x,y;Re;D/d) &= \psi_s^*(x,y;Re_c;D/d) + k_0(\Delta Re/Re_c)^{1/2}\psi_\alpha(x,y;D/d)\\ &\quad +(\Delta Re/Re_c)(\psi_1 + k_0^2\psi_{1\alpha}(x,y;D/d)) + \cdots,\\ \Omega_{as}(x,y;Re;D/d) &= \Omega_s^*(x,y;Re_c;D/d) + k_0(\Delta Re/Re_c)^{1/2}\Omega_\alpha(x,y;D/d)\\ &\quad +(\Delta Re/Re_c)(\Omega_1 + k_0^2\Omega_{1\alpha}(x,y;D/d)) + \cdots,\end{aligned}\right\} \tag{56}$$

we let

$$\psi = \psi_{as} + \epsilon\tilde{\psi}(x,y,t) + \cdots, \tag{57}$$

$$\Omega = \Omega_{as} + \epsilon\tilde{\Omega}(x,y,t) + \cdots, \tag{58}$$

where again $0 < \epsilon \ll \epsilon_\alpha$, $\tilde{\psi}$ is an unsteady stream function disturbance and $\tilde{\Omega}$ is an unsteady vorticity disturbance. Substituting the above equations into the unsteady vorticity-transport equations (2)–(4), and neglecting second-order terms, we obtain to the leading order, $O(\epsilon)$, the linearized equations of motion

$$\left.\begin{aligned}\tilde{\Omega}_t + \psi_{as_y}\tilde{\Omega}_x + \Omega_{as_x}\tilde{\psi}_y - \psi_{as_x}\tilde{\Omega}_y - \Omega_{as_y}\tilde{\psi}_x - \frac{1}{Re}(\tilde{\Omega}_{xx} + \tilde{\Omega}_{yy}) = 0,\\ \tilde{\Omega} = -(\tilde{\psi}_{xx} + \tilde{\psi}_{yy}).\end{aligned}\right\} \tag{59}$$

In studying the linearized stability problem, we consider a suitable mode analysis of (59) in the form

$$\tilde{\psi}(x,y,t) = \mathrm{e}^{\sigma t}\tilde{\phi}(x,y), \tag{60}$$

$$\tilde{\Omega}(x,y,t) = \mathrm{e}^{\sigma t}\tilde{\Phi}(x,y). \tag{61}$$

Here, in the general case, the perturbation growth rate σ may be a complex number and $\tilde{\phi}$ and $\tilde{\Phi}$ are complex functions. Substituting these expressions into (59) we obtain an eigenvalue system for solving σ, $\tilde{\phi}$, and $\tilde{\Phi}$:

$$\sigma\tilde{\Phi} + \Omega_{as_x}\tilde{\phi}_y + \psi_{as_y}\tilde{\Phi}_x - \Omega_{as_y}\tilde{\phi}_x - \psi_{as_x}\tilde{\Phi}_y - \frac{1}{Re}(\tilde{\Phi}_{xx} + \tilde{\Phi}_{yy}) = 0, \tag{62}$$

$$\tilde{\Phi} = -(\tilde{\phi}_{xx} + \tilde{\phi}_{yy}). \tag{63}$$

The boundary conditions (5)–(10) result in homogeneous conditions for $\tilde{\phi}$, $\tilde{u} = \tilde{\phi}_y$, $\tilde{v} = -\tilde{\phi}_x$, and $\tilde{\Phi}$ similar to (44) and (45).

The problem (62)–(63) with conditions (44)–(45) is an eigenvalue problem for solving the general relationship between the growth rate and Reynolds number, $\sigma(Re)$, in the asymmetric case. The solution of this problem presents a challenge and is complicated to achieve even by using numerical methods. Battaglia *et al.* (1997) and Alleborn *et al.* (1997) show only a few such computations.

It is important to observe from (62)–(63) and (22)–(23), (28)–(29) that when $Re = Re_c$, $\psi_{as} = \psi_s^*$ and, therefore, $\sigma = 0$, $\tilde{\phi} \equiv \psi_\alpha$, and $\tilde{\Phi} \equiv \Omega_\alpha$. This means that a neutrally stable mode of disturbance of the asymmetric states exists when $Re = Re_c$ and, from a dynamical perspective, it is a neutrally stable state with respect to the eigenmode ψ_α.

We concentrate on the neighbourhood of Re_c and use the following asymptotic analysis. Using the results from the previous paragraph, it is expected that as Re

approaches Re_c also $\sigma = \sigma_R + \mathrm{i}\sigma_I$ tends to zero, i.e. both the real part σ_R and the imaginary part σ_I tend to zero. Also, when Re approaches Re_c from above the asymmetric states ψ_{as}, and the related Ω_{as}, are described by the asymptotic expansions (56). Therefore, we consider the asymptotic expansions for $\tilde{\phi}$ and $\tilde{\Phi}$ in the limit as $Re \to Re_c$ from above (or $\sigma \to 0$) in the form

$$\tilde{\phi} = \psi_\alpha + \epsilon_{1R}\tilde{\phi}_{1R} + \mathrm{i}\epsilon_{1I}\tilde{\phi}_{1I} + \epsilon_{2R}\tilde{\phi}_{2R} + \mathrm{i}\epsilon_{2I}\tilde{\phi}_{2I} + \cdots, \tag{64}$$

$$\tilde{\Phi} = \Omega_\alpha + \epsilon_{1R}\tilde{\Phi}_{1R} + \mathrm{i}\epsilon_{1I}\tilde{\Phi}_I + \epsilon_{2R}\tilde{\Phi}_{2R} + \mathrm{i}\epsilon_{2I}\tilde{\Phi}_{2I} + \cdots, \tag{65}$$

where again $|\epsilon_{1R}| \gg |\epsilon_{2R}|$, $|\epsilon_{1I}| \gg |\epsilon_{2I}|$ are small parameters which depend on Re and tend to 0 as Re tends to Re_c.

Substituting (64) and (65) into (62) and (63) and using (14) and (56) results in two equations from the real and imaginary parts of (62) and (63) for the solution of $\tilde{\phi}_R$ and $\tilde{\phi}_I$:

the real part is

$$\begin{aligned}
&\sigma_R\Omega_\alpha - \sigma_I\epsilon_{1I}\tilde{\Phi}_{1I} + \cdots + 2k_0\left(\frac{\Delta Re}{Re_c}\right)^{1/2}(\psi_{\alpha y}\Omega_{\alpha x} - \psi_{\alpha x}\Omega_{\alpha y}) \\
&\quad + \epsilon_{1R}\left[\Omega^*_{s\,x}\tilde{\phi}_{1Ry} + \psi^*_{s\,y}\tilde{\Phi}_{1Ry} - \Omega^*_{s\,y}\tilde{\phi}_{1Rx} - \psi^*_{s\,x}\tilde{\Phi}_{1Ry} - \frac{1}{Re_c}(\tilde{\Phi}_{1Rxx} + \tilde{\Phi}_{1Ryy})\right] \\
&\quad + \epsilon_{2R}\left[\Omega^*_{s\,x}\tilde{\phi}_{2Ry} + \psi^*_{s\,y}\tilde{\Phi}_{2Ry} - \Omega^*_{s\,y}\tilde{\phi}_{2Rx} - \psi^*_{s\,x}\tilde{\Phi}_{2Ry} - \frac{1}{Re_c}(\tilde{\Phi}_{2Rxx} + \tilde{\Phi}_{2Ryy})\right] \\
&\quad + \epsilon_{1R}k_0\left(\frac{\Delta Re}{Re_c}\right)^{1/2}(\Omega_{\alpha x}\tilde{\phi}_{1Ry} + \psi_{\alpha y}\tilde{\Phi}_{1Ry} - \Omega_{\alpha y}\tilde{\phi}_{1Rx} - \psi_{\alpha x}\tilde{\Phi}_{1Ry}) \\
&\quad + \left(\frac{\Delta Re}{Re_c}\right)\left(\psi_{\alpha y}\Omega_{1x} + \psi_{1y}\Omega_{\alpha x} - \psi_{\alpha x}\Omega_{1y} - \psi_{1x}\Omega_{\alpha y} + \frac{1}{Re_c}(\Omega_{\alpha xx} + \Omega_{\alpha yy})\right) \\
&\quad + k_0^2\left(\frac{\Delta Re}{Re_c}\right)(\psi_{\alpha y}\Omega_{1\alpha x} + \psi_{1\alpha y}\Omega_{\alpha x} - \psi_{\alpha x}\Omega_{1\alpha y} - \psi_{1\alpha x}\Omega_{\alpha y}) + \cdots = 0,
\end{aligned} \tag{66}$$

$$\tilde{\Phi}_{1R} = -(\tilde{\phi}_{1Rxx} + \tilde{\phi}_{1Ryy}), \tag{67}$$

$$\tilde{\Phi}_{2R} = -(\tilde{\phi}_{2Rxx} + \tilde{\phi}_{2Ryy}), \tag{68}$$

and, the imaginary part is

$$\begin{aligned}
&\sigma_I\Omega_\alpha + \sigma_R\epsilon_{1I}\tilde{\Phi}_{1I} \\
&\quad + \epsilon_{1I}\left[\Omega^*_{s\,x}\tilde{\phi}_{1Iy} + \psi^*_{s\,y}\tilde{\Phi}_{1Ix} - \Omega^*_{s\,y}\tilde{\phi}_{1Ix} - \psi^*_{s\,x}\tilde{\Phi}_{1Iy} - \frac{1}{Re_c}(\tilde{\Phi}_{1Ixx} + \tilde{\Phi}_{1Iyy})\right] + \cdots = 0,
\end{aligned} \tag{69}$$

$$\tilde{\Phi}_{1I} = -(\tilde{\phi}_{1Ixx} + \tilde{\phi}_{1Iyy}). \tag{70}$$

The asymptotic relations (69) and (70) show that $\sigma_I = O(\epsilon_{1I})$. Actually, the numerical studies in § 5 demonstrate that around Re_c the imaginary part for the asymmetric states also vanishes, $\sigma_I = 0$. Therefore, in the asymptotic relations (66)–(68) the term with $\sigma_I\epsilon_{1I}$ may be neglected. The leading-order terms in (66) are those relating σ_R, $\sqrt{\Delta Re/Re_c}$, and ϵ_{1R}. After multiplying these terms by ψ_α and integrating over the flow domain A, the term related $\sqrt{\Delta Re/Re_c}$ vanishes. This means that for a consistent

behaviour $|\sigma_R| \ll \sqrt{\Delta Re/Re_c}$. Therefore, the leading-order terms related to ϵ_{1R} and $\sqrt{\Delta Re/Re_c}$ give

$$\epsilon_{1R}\left[\Omega^*_{s\,x}\tilde{\phi}_{1Ry} + \psi^*_{s\,y}\tilde{\Phi}_{1Rx} - \Omega^*_{s\,y}\tilde{\phi}_{1Rx} - \psi^*_{s\,x}\tilde{\Phi}_{1Ry} - \frac{1}{Re_c}(\tilde{\Phi}_{1Rxx} + \tilde{\Phi}_{1Ryy})\right]$$
$$= -2k_0\left(\frac{\Delta Re}{Re_c}\right)^{1/2}(\psi_{\alpha y}\Omega_{\alpha x} - \psi_{\alpha x}\Omega_{\alpha y}), \qquad (71)$$

$$\tilde{\Phi}_{1R} = -(\tilde{\phi}_{1Rxx} + \tilde{\phi}_{1Ryy}). \qquad (72)$$

Comparing (71) and (72) with (32) and (33) shows that $\epsilon_{1R}\tilde{\phi}_{1R} = 2k_0\sqrt{\Delta Re/Re_c}\psi_{1\alpha}$ and $\epsilon_{1R}\tilde{\Phi}_{1R} = 2k_0\sqrt{\Delta Re/Re_c}\Omega_{1\alpha}$. Substituting this back into (66) and collecting terms shows

$$\sigma_R\Omega_\alpha + \epsilon_{2R}\left[\Omega^*_{s\,x}\tilde{\phi}_{2Ry} + \psi^*_{s\,y}\tilde{\Phi}_{2Rx} - \Omega^*_{s\,y}\tilde{\phi}_{2Rx} - \psi^*_{s\,x}\tilde{\Phi}_{2Ry} - \frac{1}{Re_c}(\tilde{\Phi}_{2Rxx} + \tilde{\Phi}_{2Ryy})\right]$$
$$+ \left(\frac{\Delta Re}{Re_c}\right)\left[3k_0^2(\Omega_{\alpha x}\psi_{1\alpha y} + \psi_{\alpha y}\Omega_{1\alpha x} - \Omega_{\alpha y}\psi_{1\alpha x} - \psi_{\alpha x}\Omega_{1\alpha y})\right.$$
$$\left. + \psi_{\alpha y}\Omega_{1x} + \psi_{1y}\Omega_{\alpha x} - \psi_{\alpha x}\Omega_{1y} - \psi_{1x}\Omega_{\alpha y} + \frac{1}{Re_c}(\Omega_{\alpha xx} + \Omega_{\alpha yy})\right] + \cdots = 0. \qquad (73)$$

Equation (73) shows that $\sigma_R = k_{as}\Delta Re/Re_c$. Assuming that $|\epsilon_{2R}| \ll \Delta Re/Re_c$, multiplying (73) by ψ_α, integrating over the flow domain A, and using the formula (36) for k_0 results in the stability coefficient for the asymmetric states

$$k_{as} = 2\frac{\iint_A\left(\psi_{\alpha y}\Omega_{1x} + \psi_{1y}\Omega_{\alpha x} - \psi_{\alpha x}\Omega_{1y} - \psi_{1x}\Omega_{\alpha y} + \frac{1}{Re_c}(\Omega_{\alpha xx} + \Omega_{\alpha yy})\right)\psi_\alpha \,\mathrm{d}y\,\mathrm{d}x}{\iint_A(\psi^2_{\alpha x} + \psi^2_{\alpha y})\,\mathrm{d}y\,\mathrm{d}x}. \qquad (74)$$

The comparison between (74) and (55) shows that $k_{as} = -2k_s$. Since $k_s > 0$ then $k_{as} < 0$. For example, when $D/d = 3$ the asymptotic estimation gives $k_s = 0.102$ and, therefore, we find that $k_{as} = -0.204$.

The numerical dynamical simulations described in § 6 can also be used to estimate the sign and value of k_{as}. For example, when $D/d = 3$ it is found that $Re_c = 53.8$ and $k_{as} = -0.195 \pm 0.005$ which is in agreement with the predictions according to (74) and may also justify the assumption that $|\epsilon_{2R}| \ll \Delta Re/Re_c$.

The result (74) shows that the asymmetric states bifurcating at the critical Reynolds number have a decaying mode of perturbation. As Re is decreased toward the critical Reynolds number Re_c the real part of the decay rate σ of the perturbation mode (60) and (61) tends to zero. This demonstrates that for a fixed D/d the asymmetric states in the expanding channel may be stable and they lose their stability characteristics as Re is decreased toward Re_c. Equation (74) reflects that the stability of the asymmetric states is a result of the nonlinear interaction between the flow perturbations ψ_1 and ψ_α.

Equations (56), (59)–(61), (64), (65) and (73) can now be used to explain the mechanism by which the asymmetric states are stable when $Re > Re_c$. It can be seen from (59) that several major effects compete on the stability of the base asymmetric flow. These are the convection of the vorticity perturbation by the axial velocity of the base flow, the convection of the base flow vorticity by the axial flow perturbations, and

the viscous dissipation of the vorticity perturbation. Equations (56) and (59) show that the first effect is composed of (i) a downstream convection of the perturbation by the symmetric part of the base flow and (ii) an upstream convection of the perturbation on one side of the channel by the asymmetric part of the base flow. The second effect is composed of (iii) a convection of the vorticity of the symmetric part of the base flow by the perturbation and (iv) a convection of the vorticity of the asymmetric part of the base flow by the perturbation. (v) The viscous dissipation has a stabilizing effect but when $Re > Re_c$ this is a relatively small effect. The combination of these effects determines the stability of the asymmetric state. Equations (64) and (65) show that the most important perturbation is again the one related to the eigenmode ψ_α. This eigenmode also describes the asymmetric part of the base asymmetric state. Therefore, effects (i), (iii), and (v) combine together exactly as in the stability of the symmetric state. When $Re > Re_c$ this combination creates an unstable effect to initiate the growth of the asymmetric perturbation. On the other hand, effects (ii) and (iv) are similar and together create a combined convection effect of the vorticity perturbation by the axial velocity perturbation in the downstream direction. When $Re > Re_c$ this combined effect grows with the size of the perturbation and has a stabilizing influence. It helps to stabilize the growth of the asymmetric perturbation to the symmetric flow and establish the asymmetric steady state. In the neighbourhood of Re_c, the larger Re is, the more stable the asymmetric flow becomes.

4.3. *Summary of asymptotic and stability analyses around* Re_c

The results of §§ 3 and 4 are summarized in the bifurcation diagram shown in figure 5. This figure shows steady-state results according to the asymptotic solutions (shown by the solid and dashed lines) and direct numerical simulations of (1)–(10) (shown by the symbols) for the case where $D/d = 3$ (for more details on the computations, see §§ 5 and 6). In this figure we use the parameter $v_{max}(x, 0; Re, D/d)$, the maximum transverse speed along the channel centreline, as a measure of the asymmetry of a certain flow state. For the branch of symmetric states, $v_{max}(x, 0; Re, D/d) = 0$ for all Re, whereas for the branch of asymmetric states bifurcating at Re_c, $v_{max}(x, 0; Re, D/d) = k_0\sqrt{\Delta Re/Re_c}\psi_{\alpha x}(x_*, 0; D/d) + \cdots$ where x_* is the location of maximum transverse speed. The stability characteristics of the various branches of flow states are also shown in figure 5. The relationship between flow criticality and stability is evident. The transition from the unstable symmetric states to the stable asymmetric states when $Re > Re_c = 53.8$ is also understood from this figure. It can also be seen from figure 5 that when $Re < 65$ the asymptotic results for both the symmetric and the asymmetric states agree with the numerical simulations within 0.01 of U_{ave}. As Re is increased above 65, the flow asymmetries predicted by the asymptotic solutions for the primary branch are greater than those found in the numerical simulations. The reason for this deviation may be related to the second-order nonlinear effects which are neglected in the asymptotic analysis around Re_c but are included in the direct numerical simulations. These effects become important as Re increases much above Re_c. This bifurcation and stability diagram is similar to that presented in the experimental and numerical studies of Fearn *et al.* (1990) and the simulations by Battaglia *et al.* (1997).

5. Numerical scheme

5.1. *Global scheme*

The vorticity–stream function equations (1)–(10) which describe the evolution of the flow in the channel are solved numerically. A uniform finite-difference mesh with step

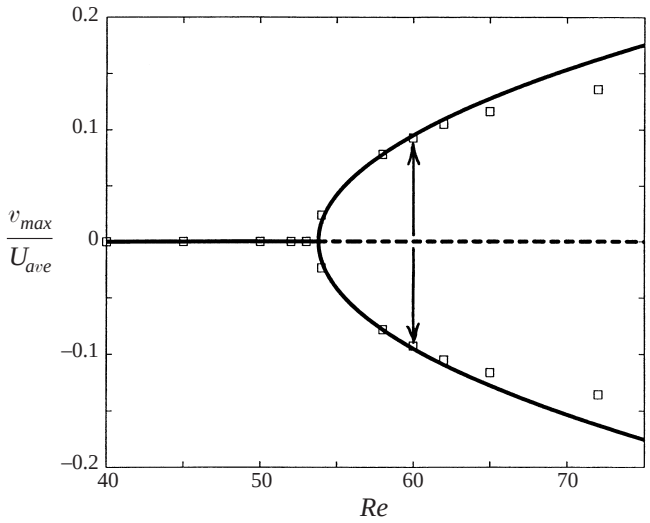

FIGURE 5. The bifurcation diagram and stability characteristics for a low-Reynolds-number flow in an expanding channel with $D/d = 3$. Lines represent asymptotic results where a solid line represents a stable solution and a dashed line represents an unstable solution. Open squares represent results from numerical simulations. The arrows represent a transition phenomenon from an unstable state to a stable state.

sizes Δx and Δy is constructed in the flow domain A with grid points labelled by (i, j), where $1 \leqslant i \leqslant IM$ and $1 \leqslant j \leqslant JM$. Equal time steps Δt are considered where each time level is labelled by n. The time-derivative term is approximated by a first-order forward-difference expression whereas second-order central-difference schemes are used for the spatial derivatives (Hoffmann & Chiang 1998). The conservative form of (2) is used for the convective terms. Therefore, the finite-difference formulation used to numerically solve equations (1)–(10) is given by a central-differences scheme:

$$\frac{\Omega_{i,j}^{n+1} - \Omega_{i,j}^{n}}{\Delta t} + \frac{u_{i+1,j}^{n}\Omega_{i+1,j}^{n} - u_{i-1,j}^{n}\Omega_{i-1,j}^{n}}{2\Delta x} + \frac{v_{i,j+1}^{n}\Omega_{i,j+1}^{n} - v_{i,j-1}^{n}\Omega_{i,j-1}^{n}}{2\Delta y}$$
$$= \frac{1}{Re}\frac{\Omega_{i+1,j}^{n} - 2\Omega_{i,j}^{n} + \Omega_{i-1,j}^{n}}{(\Delta x)^2} + \frac{1}{Re}\frac{\Omega_{i,j+1}^{n} - 2\Omega_{i,j}^{n} + \Omega_{i,j-1}^{n}}{(\Delta y)^2}. \qquad (75)$$

Here the time step is chosen such that the Courant number $C = \Delta t/\Delta x < 1.0$ and the cell Reynolds number $Re_{cell} = Re\Delta x < 2/C$ to ensure that the scheme is numerically stable. At each time level n, an iterative point-relaxation algorithm according to the Gauss–Seidel formulation is used to solve the Poisson equation (3) for the stream function (Hoffmann & Chiang 1998). The iterative process for iteration step k is given by

$$\psi_{i,j}^{n,k+1} = \frac{1}{2(1+\kappa^2)}\left[(\Delta x)^2\Omega_{i,j}^{n,k} + \psi_{i+1,j}^{n,k} + \psi_{i-1,j}^{n,k+1} + \kappa^2\left(\psi_{i,j+1}^{n,k} + \psi_{i,j-1}^{n,k+1}\right)\right]. \qquad (76)$$

Here $\kappa = \Delta x/\Delta y$. The iteration steps are repeated until for a certain k

$$\max_{i,j}\left|\psi_{i,j}^{n,k+1} - \psi_{i,j}^{n,k}\right| < \delta_\psi \qquad (77)$$

where δ_ψ is a small positive number. We use as a convergence condition $\delta_\psi = 10^{-7}$ for every time level n. It is found that changing δ_ψ to lower values only increases the number of iterations but does not affect the numerical solution of the flow dynamics.

Other flow parameters, such as speeds u and v, are computed by a second-order centred-difference approximation, i.e.

$$u_{i,j}^n = \frac{\psi_{i,j+1}^n - \psi_{i,j-1}^n}{2\Delta y}, \quad v_{i,j}^n = -\frac{\psi_{i+1,j}^n - \psi_{i-1,j}^n}{2\Delta x}. \tag{78}$$

The entire numerical scheme is explicit, first order in time and second order in space. We start from an initial state which is a perturbed symmetric solution given by

$$\left.\begin{aligned} \psi(x, y, 0; Re; D/d) &= \psi_s(x, y; Re; D/d) + \delta k_0 \psi_\alpha, \\ \Omega(x, y, 0; Re; D/d) &= \Omega_s(x, y; Re; D/d) + \delta k_0 \Omega_\alpha. \end{aligned}\right\} \tag{79}$$

The steady symmetric state $\psi_s(x, y; Re; D/d)$ and $\Omega_s(x, y; Re; D/d)$ is computed by solving the problem in the upper half of the domain, by using the symmetry boundary conditions along the x-axis at $y = 0$ for all time t, and then by reflecting the flow solution in the upper region to the lower region. The perturbation functions ψ_α and Ω_α in (79) are computed according to (30) and the size of the initial perturbation is determined by the parameter δ. The above numerical scheme is used to integrate the flow solution in space and time. The vorticity difference at each time step n is used as a measure for the convergence of the flow dynamics to steady state. The time integration is continued until

$$\max_{i,j} \left| \Omega_{i,j}^{n+1} - \Omega_{i,j}^n \right| < \delta_\Omega \tag{80}$$

where $\delta_\Omega = 10^{-10}$ is used in the present computations. Although the Poisson equation convergence is $\delta_\psi = 10^{-7}$, it typically becomes $\delta_\psi \approx 10^{-11}$ as the flow approaches a steady state.

5.2. *Computations near the expansion corners*

One of the problems in computing an accurate solution of (1)–(10) is the local singular behaviour of a viscous flow around an expansion corner with a right angle. To obtain this behaviour near the channel corners at $(x = 0, y = -1/2)$ and at $(x = 0, y = +1/2)$, we follow the analysis of Moffatt (1964) and study the flow field around a right-angle corner. The details of the asymptotic corner solution are described in the Appendix.

The asymptotic solution (A 14) and (A 16) around a right-angle corner is used in the numerical computations to establish the values of flow properties near the upper and lower expansion corners. The region of validity of the asymptotic corner solution is given by the condition (A 15). In the present numerical computations we apply this solution at the seven grid points surrounding each of the corners and denoted by $\circ$ (see figure 6). The asymptotic and numerical solutions are expected to match along the intermediate grid points, denoted by $\diamond$ (see figure 6). The two parameters $D_{\alpha_1}(t)$ and $D_{\alpha_2}(t)$ in the asymptotic solution (A 14) are computed from matching both solutions for ψ along the intermediate grid points. For example, when a uniform mesh is constructed near the expansion corner and the distance between the expansion corner and any intermediate point $\diamond$ satisfies the required condition (A 15), there are 13 relations at the intermediate points (see figure 6). Using (A 14), the relationship between the location and ψ at each of the 13 intermediate points and

at each time level $n+1$ may be described in a matrix form by

$$\boldsymbol{X}\begin{pmatrix} D_{\alpha_1}(t) \\ D_{\alpha_2}(t) \end{pmatrix}^{(n+1)} = \begin{pmatrix} \psi_1 - \psi_0 \\ \psi_2 - \psi_0 \\ \vdots \\ \psi_{13} - \psi_0 \end{pmatrix}^{(n)} \tag{81}$$

where the matrix $\boldsymbol{X}$ is given by

$$\boldsymbol{X} = \begin{pmatrix} r_1^{\alpha_1} f_{\alpha_1}(\theta_1) & r_1^{\alpha_2} f_{\alpha_2}(\theta_1) \\ r_2^{\alpha_1} f_{\alpha_1}(\theta_2) & r_2^{\alpha_2} f_{\alpha_2}(\theta_2) \\ \vdots & \vdots \\ r_{13}^{\alpha_1} f_{\alpha_1}(\theta_{13}) & r_{13}^{\alpha_2} f_{\alpha_2}(\theta_{13}) \end{pmatrix}. \tag{82}$$

Multiplying both sides of (81) from the left by the transpose matrix of $\boldsymbol{X}$, $\boldsymbol{X}^T$, we find

$$\boldsymbol{Y}\begin{pmatrix} D_{\alpha_1}(t) \\ D_{\alpha_2}(t) \end{pmatrix}^{(n+1)} = \boldsymbol{X}^T \begin{pmatrix} \psi_1 - \psi_0 \\ \psi_2 - \psi_0 \\ \vdots \\ \psi_{13} - \psi_0 \end{pmatrix}^{(n)} \tag{83}$$

where the matrix $\boldsymbol{Y}$ is given by

$$\boldsymbol{Y} = \boldsymbol{X}^T \boldsymbol{X}. \tag{84}$$

Then, multiplying both sides of (83) from the left by the inverse matrix of $\boldsymbol{Y}$, $\boldsymbol{Y}^{-1}$, we find

$$\begin{pmatrix} D_{\alpha_1}(t) \\ D_{\alpha_2}(t) \end{pmatrix}^{(n+1)} = \boldsymbol{Y}^{-1}\boldsymbol{X}^T \begin{pmatrix} \psi_1 - \psi_0 \\ \psi_2 - \psi_0 \\ \vdots \\ \psi_{13} - \psi_0 \end{pmatrix}^{(n)}. \tag{85}$$

Thus, the two parameters $D_{\alpha_1}(t)$ and $D_{\alpha_2}(t)$ can be estimated from (85) using the numerical solution at the previous time level for ψ. All the flow parameters in the region inside the intermediate points, denoted by ○, are then computed by the asymptotic solution. All the flow parameters outside this region and at the 13 intermediate points are computed by the numerical scheme (75)–(76). This is a least-squares method of solution for $D_{\alpha_1}(t)$ and $D_{\alpha_2}(t)$.

In order to further increase the accuracy of numerical results and satisfy the condition (A 15), we also introduce a multiple grid refinement near the expansion corners (see figure 7). The method for the grid refinement is based on the third-order tensor product polynomial (see Chesshire & Henshaw 1990 or Cole & Schwendeman 1990 for more details of this technique) to satisfy the consistency of the numerical scheme between the global and local grids. As *Re* of the incoming flow is increased, the region where the asymptotic corner solution is valid becomes smaller and more grid refinement levels are used. The local asymptotic solution and grid refinement are used at each time level of the numerical scheme.

6. Numerical studies

We first investigated the sensitivity of the numerical solutions to grid refinement, time-step reduction, and domain size. We concentrated on a channel with an expansion

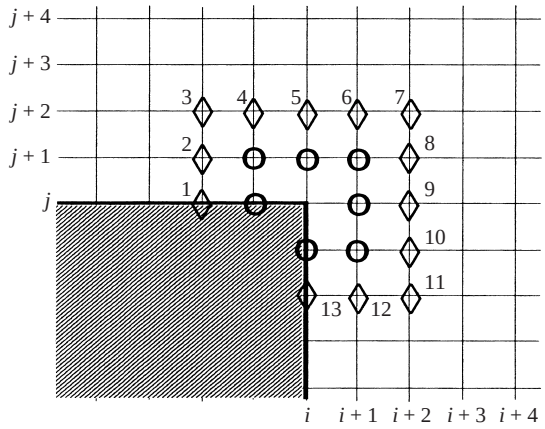

FIGURE 6. Grid geometry near an expansion corner.

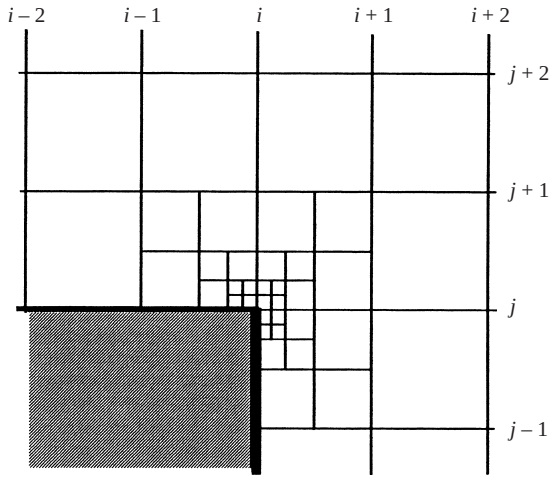

FIGURE 7. Grid refinement geometry near an expansion corner.

ratio $D/d = 3$. Two typical test cases where $Re = 40$ and $\delta = 0.16$ and $Re = 65$ and $\delta = 0.05$ were investigated in detail. Discussion on the flow dynamics in these cases is given later in this section. In the first case, the flow is initially perturbed, the disturbances decay in time, and the flow returns to a symmetric equilibrium state, whereas in the second case, the disturbance evolves into an asymmetric equilibrium state. Uniform meshes with step sizes $\Delta x = \Delta y = 0.05$ and $\Delta x = \Delta y = 0.025$ were used in the grid refinement analysis. Similar mesh step sizes were used by Fearn *et al.* (1990), Durst *et al.* (1993), Battaglia *et al.* (1997), Drikakis (1997), and Alleborn *et al.* (1997) in their Navier–Stokes simulations. Three local grid refinement levels were also used near the expansion corners such that the local mesh size near the corners is on the order of $\Delta x = \Delta y = 0.006$. We first find that for computing the time-asymptotic (steady) states, the mesh with step sizes of 0.05 provides sufficient accuracy when compared with the computations using the more refined mesh with step sizes of 0.025. The maximum absolute value of the variations of ψ at points in the flow field is less than 2% for both cases of Re. It should be pointed out, however, that local variations of about 6% were found in computing the vorticity field Ω. Similar

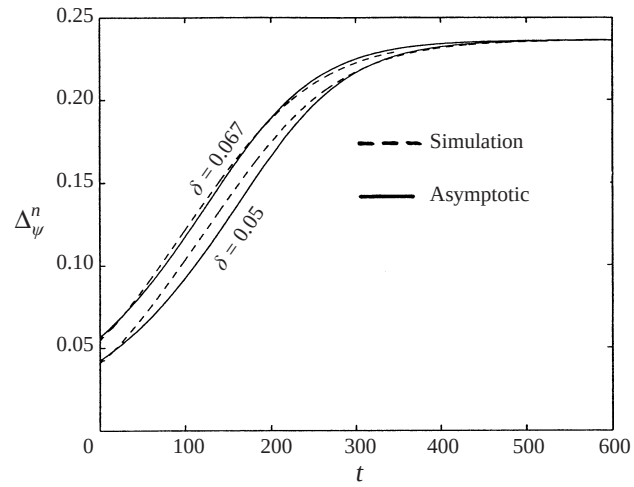

FIGURE 8. Time-history plots of the norm Δ_ψ^n for various initial disturbances according to the direct numerical simulations and the weakly nonlinear theory of Rusak & Hawa (1999) for $Re = 58$ and $D/d = 3$.

sensitivities were found in the simulations of Battaglia *et al.* (1997) and Alleborn *et al.* (1997). It should also be emphasized here that a good correlation is found between the decay or growth rates of small disturbances and the theoretical predictions found in § 4. Moreover, the time-asymptotic states of the present simulations show agreement with the asymptotic predictions for every Re in the range $1 \leqslant Re < 65$ (see figure 5 above). These issues provide additional confidence in the present computations.

The numerical stability condition on the cell Reynolds number, $Re_{cell} < 2/C$ with $C = \Delta t/\Delta x < 1$, typically dictates the time step size Δt. Therefore, as Re decreases smaller time steps should be used. For example, when $Re = 65$ a time step $\Delta t = 0.0008$ is used and when $Re = 40$ a time step $\Delta t = 0.0005$ is used. Numerical results for the above-mentioned meshes and test cases showed similar evolution of the flow fields when even smaller time steps were used. In addition, figure 8 presents time-history plots of the maximum difference of the temporal solution from the symmetric state, defined as $\Delta_\psi^n = \max_{i,j}(|\psi_{i,j}^n - \psi_{si,j}|)$, for the cases where $Re = 58$, $D/d = 3$, and $\delta = 0.067, 0.05$. The uniform mesh for both cases has step sizes $\Delta x = \Delta y = 0.05$. Also shown in figure 8 are results of the flow dynamics according to the weakly nonlinear theory of Rusak & Hawa (1999). It can be seen that the flow evolution according to the direct numerical simulations and the asymptotic predictions agree one with the other. We also refer to figures 3, 4, and 5 in Rusak & Hawa (1999) for additional comparisons of results from the numerical simulations with the weakly nonlinear theory predictions. Agreement between these results was found for all cases where Re is around $Re_c = 53.8$ and $\delta > 0.04$. The differences between results for cases where Re is away from Re_c can be attributed to the second-order terms that become important for such Re but are neglected in the weakly nonlinear analysis. However, it should be pointed out here that for cases where Re is close to Re_c (such as $Re = 58$) and where the initial perturbation is relatively small, $\delta < 0.02$, global mesh refinement is needed in order to capture the details of the relatively slow flow dynamics (see figure 5 in Rusak & Hawa 1999). Despite this, the time-asymptotic (steady) states for these cases can be still accurately computed with coarser meshes.

Our experience also shows that the flow dynamics is not affected when the channel

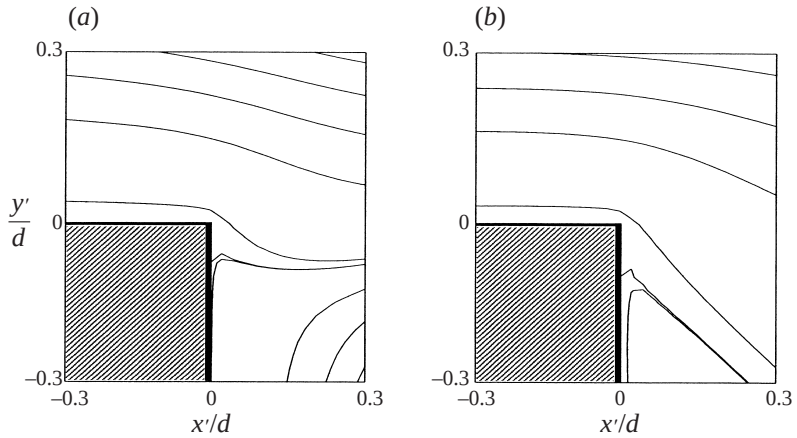

FIGURE 9. Streamline patterns of the local flow around the corner for $Re = 5$ according to (a) the asymptotic formula (A 14), and (b) the numerical simulation including the matching with (A 14).

inlet section is at $-x_0 \leqslant -2.0$. On the other hand, the outlet section at x_1 should be carefully chosen to ensure fully developed laminar flow at the outlet, specifically as Re increases. We find that the flow dynamics is not affected by the outlet conditions in the range $10 < Re < 100$ when $x_1 \geqslant 40$.

These results demonstrate the numerical accuracy of the present computations as both the mesh and time step sizes are decreased and the size of the computational domain is increased.

A typical local behaviour of the flow near the expansion corner for the case where $Re = 5$ (symmetric channel flow) is presented in figure 9. We find that this flow solution near the corners does not change with mesh refinement as long as the condition (A 15) is satisfied. When $Re = 5$ only one level of refinement is needed to achieve a converged solution. The computations show that at the steady state $D_{\alpha_1} = 0.74\cdots$ and $D_{\alpha_2} = -0.25\cdots$. The streamline patterns of the flow for this case according to the asymptotic formula (A 14) are described in figure 9(a) and the flow solution including the matching with the asymptotic formula (A 14) is described in figure 9(b). It can be seen that when $Re = 5$ the smooth asymmetric mode dominates the flow near the corners in both the asymptotic corner solution and the numerical simulation. The separation region develops along the vertical wall, at about $0.1d$ away from the corner. As Re increases, the separation region approaches the corner and when $Re > 30$ it develops very close to the corner.

To demonstrate the advantage of using the present numerical scheme with the asymptotic corner solution, we also conducted numerical simulations with the same finite-difference scheme without the local corner solution. In this second (standard) scheme, the derivatives at the grid points just around the corners were calculated using second-order backward differences (at points upstream of the corners) or second-order forward differences (at points downstream of the corners). In this way, we avoid the need to compute the values of Ω at the corners. The second scheme also used the same meshes as well as the same mesh refinement technique around the corners as described above. The results of the streamline patterns around the corners according to the standard scheme for $Re = 5$ are compared in figure 10 with the results according to the present scheme. It can be seen that, unlike the present numerical method, the standard scheme needs several levels of refinement near the corners (at least 5 levels) to achieve

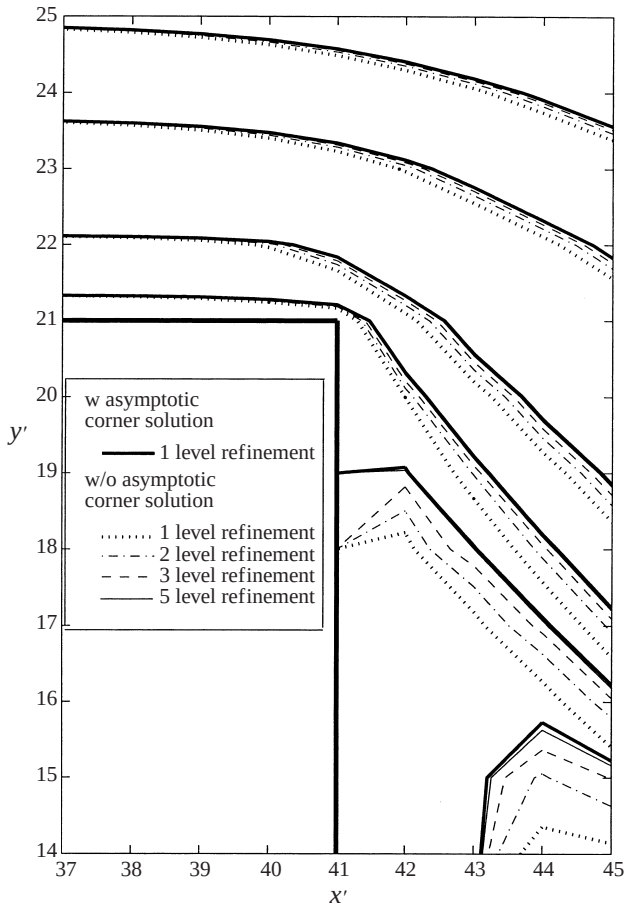

FIGURE 10. Comparison of streamline patterns according to the numerical scheme using the asymptotic corner solution and a standard scheme with different levels of refinement for $Re = 5$.

numerical convergence of the solution near the corners. Moreover, it is very interesting to see that the results of the standard scheme converge toward the results of the present scheme as the level of refinement is increased. These computations demonstrate that the use of the local corner solution within the numerical simulation of the flow in the channel enhances the accuracy of the simulations and requires less computational effort (refinements near the corners) to achieve converged numerical results.

The present numerical computations are also compared with the experimental measurements reported in Fearn *et al.* (1990) of the axial velocity fields at various cross-sections along a channel with an expansion ratio $D/d = 3$. Figure 11(*a*) shows the results for the case $Re = 40$ where the flow is symmetric and figure 11(*b*) shows results for the case $Re = 80$ where the flow establishes an asymmetric state. It can be seen from both figures that the present numerical computations provide a good prediction of the flow fields in both cases, similar to the simulations of Fearn *et al.* (1990), Durst *et al.* (1993), Drikakis (1997), and Battaglia *et al.* (1997).

The dynamics of several flow cases with various incoming Reynolds numbers in a channel with an expansion ratio $D/d = 3$ is now studied. For this channel geometry, the numerical analyses of Battaglia *et al.* (1997) show that $Re_c = 53.8$.

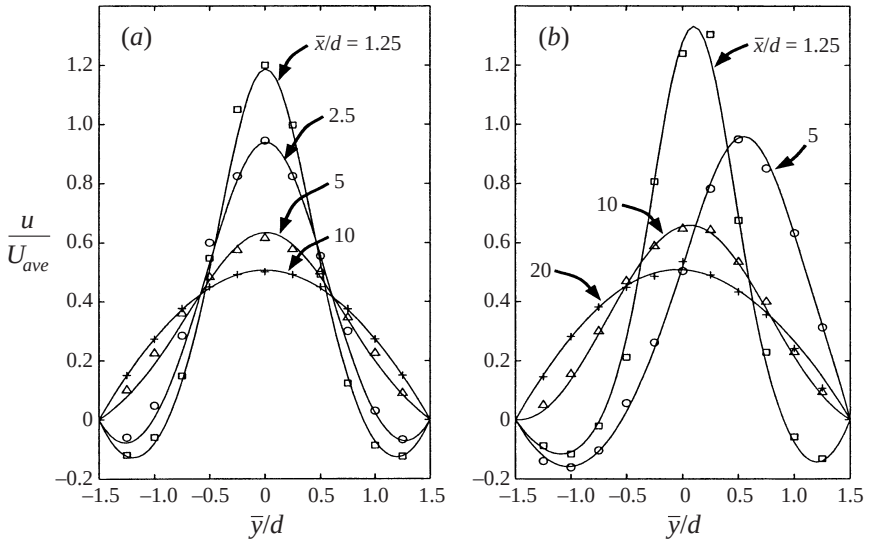

FIGURE 11. Comparison of computational results with experimental axial flow measurements by Fearn *et al.* (1990) at various cross-sections along a channel with $D/d = 3$ when (*a*) $Re = 40$ and (*b*) $Re = 80$.

A similar result is also found in Drikakis (1997), Alleborn *et al.* (1997), and the present results described below. The initial perturbation functions $k_0\psi_\alpha$ and $k_0\Omega_\alpha$ in (79) are calculated using (30) (where the symmetric and asymmetric equilibrium states computed at $\widetilde{Re} = 54$ are used in (30)).

In the first case, we study a flow with $Re = 40$. In this case, $Re < Re_c$ and, according to the theory, the base symmetric state is unconditionally stable to any two-dimensional disturbance. Starting from the initial conditions (79) with $\delta = 0.16$ we can see in figure 12 that even a large asymmetric disturbance decays relatively quickly. After about 100 time units, d/U_{ave}, the flow returns to a symmetric state and stays there as expected. Similar behaviour occurs with any other disturbance value of δ and the only difference is the time it takes for a disturbance to decay, which is a function of the size of the initial amplitude δ.

Figure 13 shows lines of $\psi(x, y, t; Re; D/d) - \psi_s(x, y; Re; D/d)$ along horizontal cross-sections of the channel at $y = \pm 1.0$ and at various times. Again, it can be seen that the initial asymmetric perturbation quickly decays in time. The decay process seems to be related to the viscous dissipation and also to the slight effect of the convection of the perturbation by the axial velocity of the base symmetric flow. This mechanism of decay matches the predictions from the stability study in § 4.1.

To demonstrate the absolute decay to a symmetric state when $Re = 40$, we show the time-history plots of the norm Δ_ψ^n (see figure 14). It can be seen that for the two cases with $Re = 40$ and $\delta = 0.008$ (a small initial perturbation) or $\delta = 0.16$ (a large initial perturbation), the dynamics of the disturbance is similar: after a nonlinear transient and when the perturbation becomes sufficiently small, Δ_ψ^n decays exponentially, $\Delta_\psi^n \sim \exp(\sigma_{Rs} t)$, and with almost the same rate of decay for both values of δ. For $Re = 40$, we find $\sigma_{Rs} \sim -(0.042 \pm 0.001) U_{ave}/d$.

Also shown in figure 14 are the time-history plots of the norm Δ_ψ^n for other values of Reynolds number below the critical value $Re_c = 53.8$ with same initial amplitude, $\delta = 0.008$. The comparison between the various lines shows that the decay rate of a

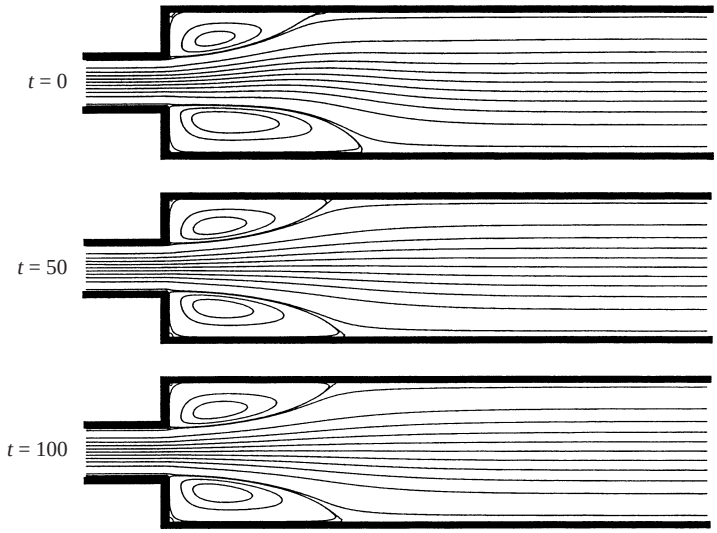

FIGURE 12. Time-history plots of the stream function $\psi(x, y, t)$ for a flow with $Re = 40$ in a channel with $D/d = 3$ and $\delta = 0.16$.

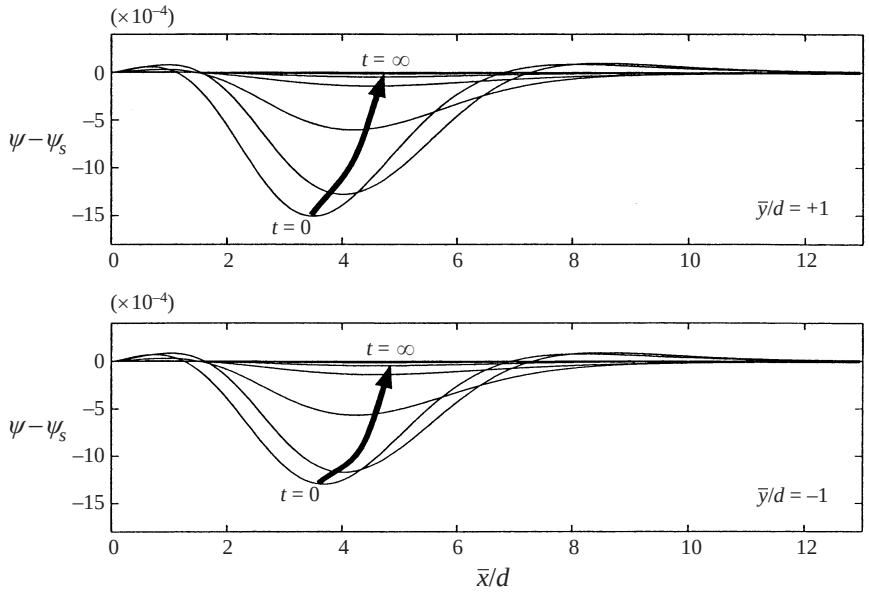

FIGURE 13. Lines of $\psi(x, y, t; Re; D/d) - \psi_s(x, y; Re; D/d)$ along horizontal cross-sections of the channel at $y = \pm 1$ for $Re = 40$, $D/d = 3$, and $\delta = 0.16$.

disturbance decreases as Re is increased toward the critical value, in accordance with the theoretical predictions of the stability study in §4.1. Moreover, when Re is very close to Re_c, we can see the very slow decay of the perturbation when $Re = 53.0$, almost no decay or growth of the perturbation when $Re = 53.8$, and the slow growth of the perturbation when $Re = 55.0$. These results clearly demonstrate the critical nature of the flow state at $Re = 53.8$ and the change of σ_{Rs} from negative to positive for the branch of symmetric states as Re is increased across $Re = 53.8$.

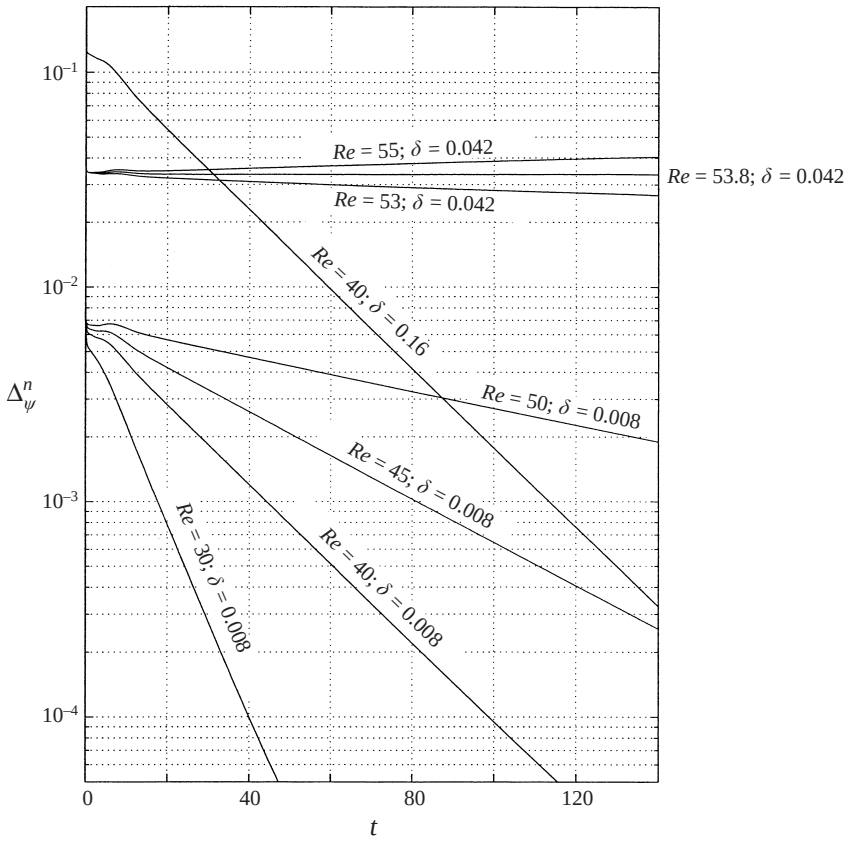

FIGURE 14. Time-history plots of the norm Δ^n_ψ for various flows with Re below and around Re_c in a channel with $D/d = 3$. Initial disturbance amplitude is indicated in each case.

We study now a flow with $Re = 65$. In this case, $Re > Re_c$ and, according to the theory, the symmetric state is unstable to two-dimensional disturbances. Starting from the initial conditions (79) with $\delta = 0.05$ we can see (figure 15) that the relatively small initial asymmetric disturbance grows in time and evolves in a nonlinear process into an asymmetric state which reaches a steady state (after about 300 time units), as expected by the stability study in §§ 4.1 and 4.2. Similar behaviour occurs with other disturbance amplitudes δ but the time it takes for a disturbance to grow and stabilize is longer with the decrease of δ.

Figure 16 presents lines of $\psi(x, y, t; Re; D/d) - \psi_s(x, y; Re; D/d)$ along horizontal cross-sections of the channel at $y = \pm 1.0$ and at various times. It can be seen again that the asymmetric initial perturbation grows in time and on one side of the channel it propagates upstream. The disturbance stabilizes at a certain position close to the expansion section. It seems that the growth of the asymmetric perturbation results from the upstream convection of the vorticity of the base symmetric state by the perturbation itself on one side of the channel. As the perturbation grows, it reaches a steady value due to the interaction of the perturbation with itself, with the inlet flow, and with the expansion corners. An asymmetric equilibrium state is established. This mechanism of disturbance growth matches the predictions from the stability studies in §§ 4.1 and 4.2.

To demonstrate the instability of the symmetric state at $Re = 65$ to various initial

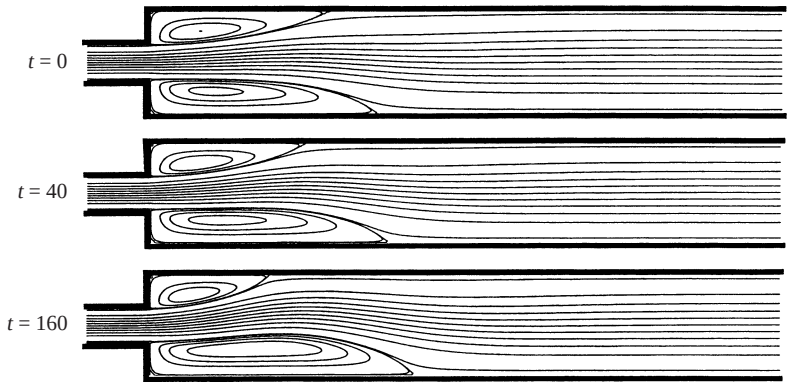

FIGURE 15. Plots of the stream function $\psi(x, y, t)$ at different times for a flow with $Re = 65$ in a channel with $D/d = 3$ and $\delta = 0.067$.

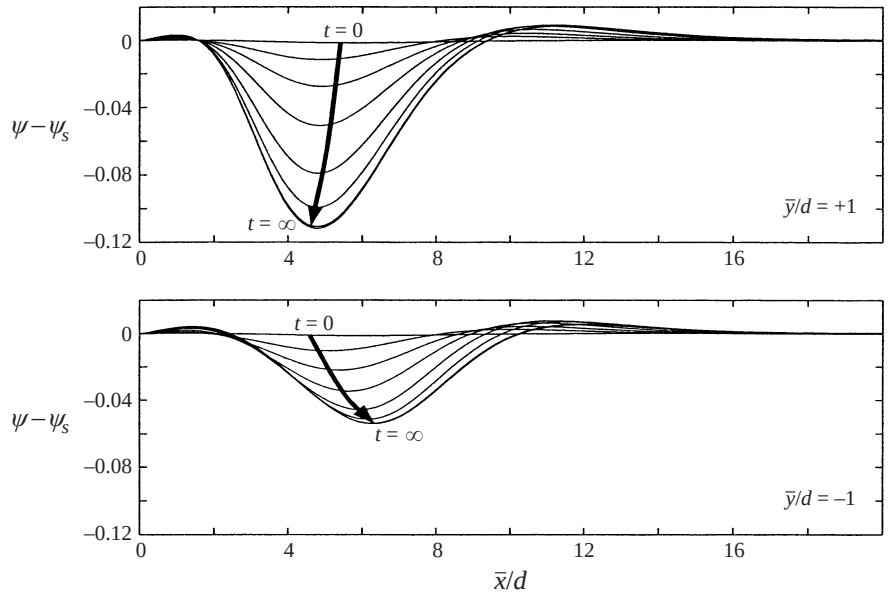

FIGURE 16. Lines of $\psi(x, y, t; Re; D/d) - \psi_s(x, y; Re; D/d)$ along horizontal cross-sections of the channel at $y = \pm 1$ for $Re = 65$ and $D/d = 3$.

disturbances and the convergence to the same steady and stable asymmetric state, time-history plots of the norm of the solution Δ_ψ^n are presented in figure 17. The growth of the perturbation in time, the significant departure from the symmetric state, and the evolution to the same asymmetric state are evident for all cases. Moreover, when the initial perturbation is not related to the eigenmode ψ_α, this disturbance quickly decays and the flow creates the mode of instability related to ψ_α. It can also be seen that for all cases with $Re = 65$ the dynamics of the disturbance is similar: the asymmetric perturbation grows exponentially, $\mathrm{d}\Delta_\psi^n/\mathrm{d}t \sim \exp(\sigma_{Rs} t)$, and with almost the same rate of growth, $\sigma_{Rs} \sim (0.015 \pm 0.002) U_{ave}/d$. The convergence to the asymmetric state is also exponential, $\mathrm{d}\Delta_\psi^n/\mathrm{d}t \sim \exp(\sigma_{Ras} t)$ and with a rate of decay, $\sigma_{Ras} \sim -(0.031 \pm 0.002) U_{ave}/d$. Note that for $Re = 65$, $\sigma_{Ras} \sim -2\sigma_{Rs}$ as predicted by the stability study in § 4.

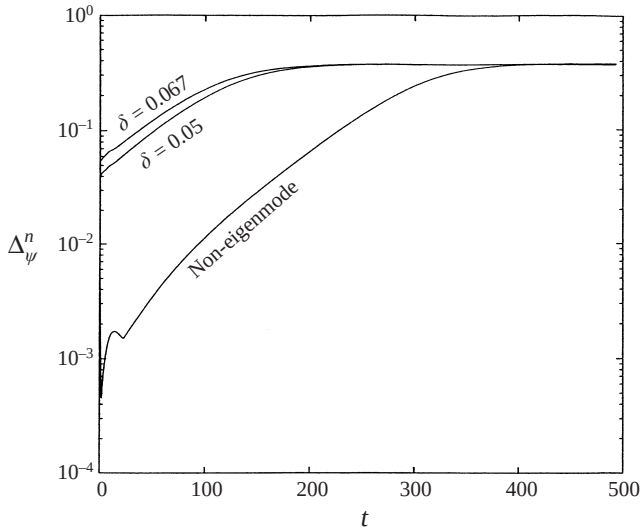

FIGURE 17. Time-history plots of the norm Δ_ψ^n for a flow with $Re = 65$ in a channel with $D/d = 3$. Initial disturbance amplitude is indicated in each case.

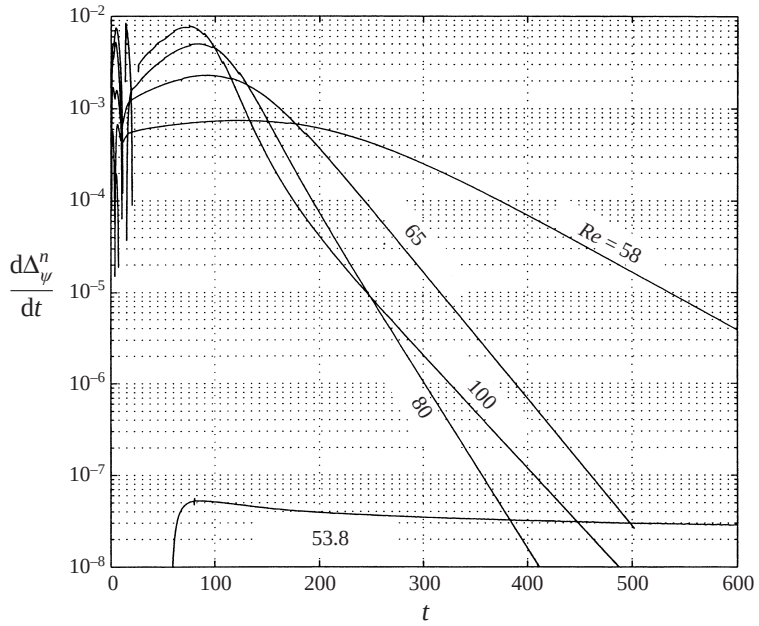

FIGURE 18. Time-history plots of the norm $d\Delta_\psi^n/dt$ for various flows with $Re > Re_c$ in a channel with $D/d = 3$. Reynolds number is indicated in each case.

Figure 18 shows time-history plots of the norm $d\Delta_\psi^n/dt$ for various values of Reynolds number above the critical value $Re_c = 53.8$ with same initial disturbance of $\delta = 0.067$. The comparison between the lines shows that the growth rate of the disturbance increases as Re is increased above the critical value, again in accordance with the theoretical predictions in § 4. It is also clear that when Re is close to 53.8, the rate of change of the disturbance tends to zero, demonstrating that the critical state

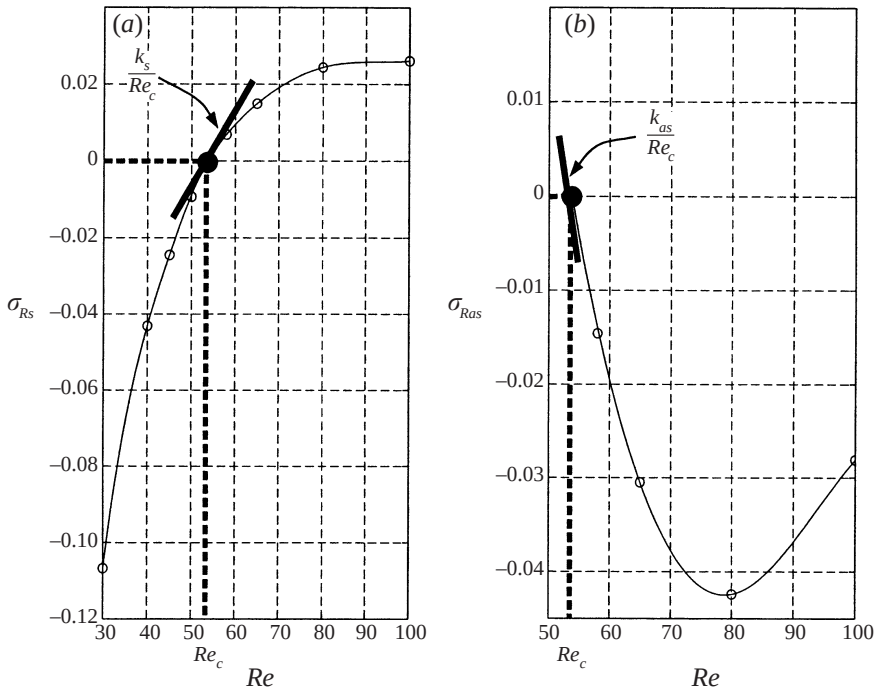

FIGURE 19. Growth rates of (*a*) the symmetric and (*b*) asymmetric states as a function of Re for a channel with $D/d = 3$.

at $Re_c = 53.8$ is a neutral state for the branch of both the symmetric and asymmetric states, i.e. $\sigma_{Rs} = \sigma_{Ras} = 0$ at $Re = 53.8$.

The time-history plots in figures 14 and 18 provide information with which to compute the decay or growth rates of disturbances, σ_{Rs} for the symmetric states, and σ_{Ras} for the asymmetric states, as function of Re for a fixed expansion ratio $D/d = 3$. The results are summarized in figure 19. It can be seen that σ_{Rs} grows monotonically with Re and $\sigma_{Rs} = 0$ at the critical state where $Re = Re_c = 53.8$, in complete agreement with Battaglia *et al.* (1997), Drikakis (1997), and Alleborn *et al.* (1997) when the same definition of Re is used. Moreover, $\sigma_{Rs} < 0$ when $Re < Re_c$ and $\sigma_{Rs} > 0$ when $Re > Re_c$. The rate of change of σ_{Rs} with $\Delta Re/Re_c$ at the critical state is computed and we find $k_s = \sigma_{Rs}/(\Delta Re/Re_c) = 0.105 \pm 0.002$ when $D/d = 3$. This value is in good agreement with the value $k_s = 0.102$ found according to the formula (55).

Figure 19 also shows that the rate σ_{Ras} is negative when $D/d = 3$ for all $Re_c < Re < 100$. The rate of change of σ_{Ras} with $\Delta Re/Re_c$ at the critical state is computed and we find $k_{as} = \sigma_{Ras}/(\Delta Re/Re_c) = -(0.195 \pm 0.005)$ when $D/d = 3$. This value is in agreement with the value $k_{as} = -2k_s = -0.204$ found according to the formula (74). Notice that nonlinear effects become important as Re increases above 65, σ_{Ras} reaches a minimum value at $Re = 77$, and it is less negative for higher values of Re.

Finally, the comparison of the streamline plots from the direct numerical simulations and the asymptotic solutions (56) at various $Re > Re_c$ is shown in figure 20. The streamline plots from the asymptotic solutions are found by using

$$\psi_{as} = \psi_s + \sqrt{\Delta Re/Re_c}(k_0\psi_\alpha),$$

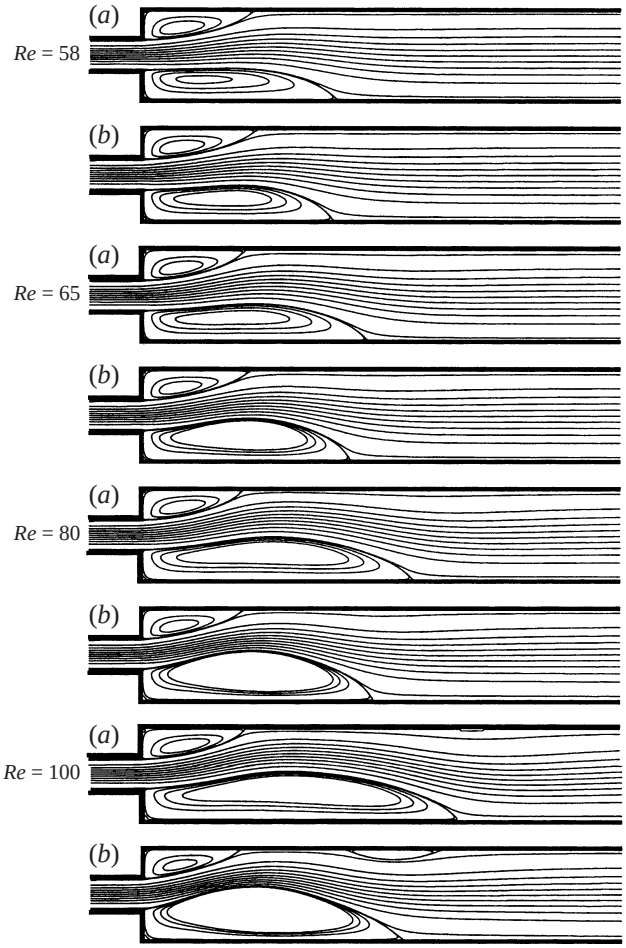

FIGURE 20. Comparison of the streamline plots from (*a*) the numerical simulations and (*b*) the asymptotic solutions at $Re = 58$, 65, 80 and 100 for a channel with $D/d = 3$.

where $(k_0\psi_\alpha)$ is computed by (30) at $\widetilde{Re} = 58$:

$$k_0\psi_\alpha = \frac{\psi_{as}(\widetilde{Re} = 58) - \psi_s(\widetilde{Re} = 58)}{\sqrt{4.2/53.8}}.$$

It can be seen that at $Re = 58$ and $Re = 65$ the streamline plots of the asymptotic solutions agree with those of the numerical simulations (see also figure 5 which is based on the same simulations for a quantitative agreement of the results). However, as Re is increased, the asymptotic solutions present more-asymmetric flow states than the numerical simulations. This may happen because of the higher-order nonlinear effects which are neglected in the asymptotic solution (56) but are included in the simulations and become dominant as Re is increased much above Re_c. In other words, as Re is increased, $\max[k_0\psi_\alpha]$ of asymptotic solutions grows like $\sqrt{Re - Re_c}$. However, $\max[k_0\psi_\alpha]$ of the numerical simulations does not grow so much with Re.

It is also interesting to notice that at $Re = 100$ both streamline plots show an additional (third) recirculation zone. The third zone predicted from the asymptotic solutions (56) is larger than that found in the direct numerical simulations. The

asymptotic solution (56) at $Re = 100$ actually shows that the eigenmode ψ_α may contain the information to create the additional recirculation zone. The appearance of the additional recirculation zone depends on the size of the amplitude of the eigenmode ψ_α. The previous experimental and numerical studies focused their attention on the size and location of the observable recirculation zones. However, the present study shows that the appearance of the additional recirculation zone probably does not result from another bifurcation point of this channel flow problem.

7. Conclusions

The dynamics of a two-dimensional viscous flow in a symmetric long channel with a sudden expansion with right angles has been studied by asymptotic analyses, linear stability studies, and numerical simulations. The bifurcation analysis of solutions of the steady Navier–Stokes equations examines the equilibrium states around a critical Reynolds number, Re_c. Asymmetric states appear in addition to the basic symmetric states when $Re \geqslant Re_c$. It is found that the bifurcation of asymmetric states at Re_c has a pitchfork nature and the asymmetric perturbation grows in a parabolic manner near Re_c. The stability analysis is based on a linearized set of the equations of motion for the development of infinitesimal two-dimensional disturbances imposed on the steady symmetric as well as asymmetric states. It is found that a neutrally stable asymmetric mode of disturbance exists at the critical state for both the symmetric and the asymmetric equilibrium states. Using asymptotic methods, it is demonstrated that the symmetric states change their stability characteristics as the Reynolds number changes around the critical level. When $Re < Re_c$ an asymptotically stable mode is found and when $Re > Re_c$ an unstable mode of disturbance may develop. It is also shown that when $Re > Re_c$, the asymmetric states have an asymptotically stable mode of disturbance. The study demonstrates that the eigenfunction ψ_α governs both the bifurcation and stability of the symmetric and asymmetric branches of flow states around Re_c. Moreover, when $Re > Re_c$, the growth rate of the instability of the symmetric states is related to the decay rate of the perturbations to the asymmetric state, i.e. $k_{as} = -2k_s$.

The direct numerical simulations based on the unsteady Navier–Stokes equations can be used to describe the evolution of a perturbed laminar, incompressible and two-dimensional flow in a suddenly expanding channel. It should be emphasized that the use of the asymptotic corner solution in the numerical simulation helps to improve the accuracy of the computations and reduce the levels of refinement needed to better resolve the flow around the corners compared to standard numerical techniques. The simulations demonstrate the relationship between the linear stability results and the time-asymptotic behaviour of the flow as described by the asymptotic steady-state solution. It is found that, indeed, the symmetric flows with $Re < Re_c$ are linearly stable to two-dimensional disturbances, whereas the symmetric states with $Re > Re_c$ are unstable. It is also interesting to notice that the rate of decay or growth of disturbances computed from the numerical simulations matches with the linear stability formulae. This result clarifies the relationship between the bifurcation/linear stability analyses and the direct numerical simulations.

The numerical studies also shed light on the nonlinear dynamics of the laminar flows in a channel with a sudden expansion and connect the bifurcation and stability analyses. It is demonstrated through the dynamics of small- and large-amplitude disturbances that the symmetric states may be absolutely stable (to any size of initial disturbance) when $Re < Re_c$ and are absolutely unstable when $Re > Re_c$. The flow

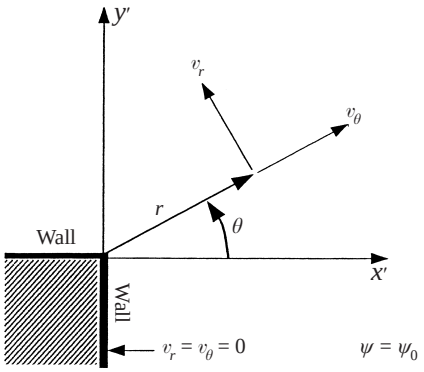

FIGURE 21. Local polar coordinate system at the lower expansion corner.

evolves into asymmetric states that may be absolutely stable when $Re > Re_c$ but lose their stability characteristics as Re approaches Re_c. From this perspective, the critical state at Re_c is a point of exchange of stability for both the symmetric and asymmetric states. This dynamical behaviour is similar to that described in the experiments of Durst *et al.* (1974), Cherdron *et al.* (1978), Fearn *et al.* (1990) and Durst *et al.* (1993).

The above asymptotic analyses and numerical simulations present an interesting physical picture of the dynamics of disturbances in a laminar flow in an expanding channel. When the Reynolds number is sufficiently low the flow cannot sustain any disturbance and any initial disturbance decays through viscous dissipation. As the Reynolds number is increased, the viscous dissipation is reduced and the symmetric flow becomes less stable. There exists the critical level Re_c where there is a critical balance between the destabilizing upstream convection effects of asymmetric perturbations and the combined stabilizing effects of the viscous dissipation and of the downstream convection of perturbations by the base flow. At this Reynolds number the flow can sustain a neutrally stable, asymmetric, standing, infinitesimal disturbance wave, the shape of which is described by the eigenfunction ψ_α. When Re is increased above Re_c the upstream convection effects of the asymmetric perturbation become dominant and, therefore, the symmetric flow becomes unstable. The larger Re is, the more unstable the symmetric flow becomes. As the asymmetric perturbation grows, the convection of the vorticity perturbation by the axial velocity perturbation creates a stabilizing influence which stops the growth of the asymmetric perturbation and establishes the asymmetric steady state. Around Re_c, the larger Re is, the more stable the asymmetric flow becomes. The asymptotic and numerical studies support this physical mechanism of transition of laminar flows in an expanding channel from symmetric to asymmetric equilibrium states.

It should be emphasized that the present analysis is limited to the study of two-dimensional disturbances. Three-dimensional disturbances may also exhibit instabilities and may dominate the flow. However, the experiments of Sobey (1985) demonstrate that for channels with a moderate expansion ratio, $D/d \sim 3$, such instabilities appear at Reynolds numbers which are much higher than $Re_c(D/d)$ for the two-dimensional disturbances.

Appendix. Local corner analysis

The asymptotic analysis around the corners follows the paper by Moffatt (1964). The flow field around a right-angle corner is studied using a polar coordinate system (r, θ), where $r = \sqrt{x'^2 + y'^2}$, $\theta = \arctan(y'/x')$ (see figure 21). Here $x' = \bar{x}/d$ and

$y' = \bar{y}/d$. The point $r = 0$ is at the expansion corner and the line $\theta = 0$ is parallel to x-axis toward downstream. In this coordinate system equations (2)–(4) take the form

$$\Omega_t + v_r\Omega_r + \frac{v_\theta}{r}\Omega_\theta = \frac{1}{Re}\left(\Omega_{rr} + \frac{1}{r}\Omega_r + \frac{1}{r^2}\Omega_{\theta\theta}\right), \tag{A 1}$$

$$\Omega = -\left(\psi_{rr} + \frac{1}{r}\psi_r + \frac{1}{r^2}\psi_{\theta\theta}\right), \tag{A 2}$$

$$v_r = \frac{1}{r}\psi_\theta, \quad v_\theta = -\psi_r, \tag{A 3}$$

where $v_r(r, \theta, t)$ and $v_\theta(r, \theta, t)$ denote the velocity components in the radial and circumferential directions, respectively (see figure 21).

The boundary conditions are the tangency and no-slip conditions at the walls as well as the behaviour of the outer solution as r increases. For example, for the lower expansion corner (at $x = 0, y = -1/2$), at all time t the conditions are

$$\left.\begin{aligned} v_r(r, \theta = \pi, t) = 0, \quad v_\theta(r, \theta = \pi, t) = 0, \\ v_r(r, \theta = -\pi/2, t) = 0, \quad v_\theta(r, \theta = -\pi/2, t) = 0. \end{aligned}\right\} \tag{A 4}$$

We look for a local solution around the expansion corner in the small region, $0 < r \ll 1$. We expect that for all time t, the stream function variations near the corner are relatively small. Therefore, according to Moffatt (1964) for all time t the stream function $\psi(r, \theta, t)$ may be given by the asymptotic expansion

$$\psi(r, \theta, t) = \psi_0 + r^\alpha F_\alpha(\theta, t) + r^\beta F_\beta(\theta, t) + \cdots \tag{A 5}$$

where ψ_0 is a constant reference stream function at the wall. Using (A 5), the velocity components $v_r(r, \theta, t)$ and $v_\theta(r, \theta, t)$ can be computed, and, for finite speeds near the corner, $\alpha > 1$.

Substituting (A 5) into (A 1)–(A 3) and neglecting the higher-order time-derivative terms and convective terms in the vorticity transport equation, results in the leading order $O(r^{\alpha-4})$ equation:

$$F_{\alpha\theta\theta\theta} + (\alpha^2 + (\alpha - 2)^2)F_{\alpha\theta\theta} + \alpha^2(\alpha - 2)^2 F_\alpha = 0. \tag{A 6}$$

This equation means that the flow near the corner behaves like a Stokes flow (very viscous flow) for which $\nabla^2\Omega = 0$. When $\alpha = 2$, the solution of (A 6) is

$$F_2(\theta, t) = A_2 \sin(2\theta) + B_2 \cos(2\theta) + C_2\theta + D_2 \tag{A 7}$$

and when $1 < \alpha \neq 2$, the solution is

$$F_\alpha(\theta, t) = A_\alpha \sin(\alpha\theta) + B_\alpha \cos(\alpha\theta) + C_\alpha \sin((\alpha - 2)\theta) + D_\alpha \cos((\alpha - 2)\theta). \tag{A 8}$$

It should be clarified that the parameters A_α, B_α, C_α, and D_α in (A 8) may be functions of time t. The relations between these parameters are determined from the wall boundary conditions (A 4) according to the eigenvalue problem

$$\begin{pmatrix} \sin(\alpha\pi) & \cos(\alpha\pi) & \sin(\alpha\pi) & \cos(\alpha\pi) \\ \alpha\cos(\alpha\pi) & -\alpha\sin(\alpha\pi) & (\alpha-2)\sin(\alpha\pi) & -(\alpha-2)\cos(\alpha\pi) \\ -\sin(\alpha\pi/2) & \cos(\alpha\pi/2) & \sin(\alpha\pi/2) & -\cos(\alpha\pi/2) \\ \alpha\cos(\alpha\pi/2) & \alpha\sin(\alpha\pi/2) & -(\alpha-2)\sin(\alpha\pi/2) & -(\alpha-2)\cos(\alpha\pi/2) \end{pmatrix} \times \begin{pmatrix} A_\alpha \\ B_\alpha \\ C_\alpha \\ D_\alpha \end{pmatrix} = \begin{pmatrix} 0 \\ 0 \\ 0 \\ 0 \end{pmatrix}. \tag{A 9}$$

For a non-trivial solution of (A 9), the determinant of the influence matrix must vanish. Four distinguished values of the power α are found:

$$\alpha_0 = 1, \quad \alpha_1 = 1.5444837368\cdots, \quad \alpha_2 = 1.9085291895\cdots, \quad \alpha_3 = 2. \tag{A 10}$$

We analyse now the four cases.

Using the previous analysis, the power α must be greater than 1 and, therefore, the eigenvalue $\alpha_0 = 1$ is not relevant.

For the case $\alpha_3 = 2$, the solution (A 7) is used. Applying the four boundary conditions (A 4), the solution of (A 9) is the trivial case $A_2 = B_2 = C_2 = D_2 = 0$, where subscript 2 denotes $\alpha = 2$. Therefore, we find that the eigenvalue $\alpha_3 = 2$ is also not relevant.

Under the given geometry and flow conditions the leading-order power α must be either $\alpha_1 = 1.5444837368\cdots$ or $\alpha_2 = 1.9085291895\cdots$. The leading-order power may be $\alpha_1 = 1.5444837368\cdots$. This solution agrees with Moffatt (1964). Using the order balance of the equation of motion and the fact that both $\alpha_2 - 4 < \alpha_1 - 2$ and $\alpha_2 - 4 < 2\alpha_1 - 4$, we find that in the expansion (A 5) $\beta = \alpha_2$. This indicates that the second-order term in (A 5) is also governed by the viscous effects only. As a result, as r tends to zero

$$\psi = \psi_0 + D_{\alpha_1} r^{\alpha_1} f_{\alpha_1}(\theta) + D_{\alpha_2} r^{\alpha_2} f_{\alpha_2}(\theta) + \cdots \tag{A 11}$$

where for $i = 1, 2$ we define

$$f_{\alpha_i}(\theta) = \frac{A_{\alpha_i}}{D_{\alpha_i}} \sin(\alpha_i\theta) + \frac{B_{\alpha_i}}{D_{\alpha_i}} \cos(\alpha_i\theta) + \frac{C_{\alpha_i}}{D_{\alpha_i}} \sin((\alpha_i - 2)\theta) + \cos((\alpha_i - 2)\theta). \tag{A 12}$$

Using the eigenvalue problem (A 9) we find the relations between the various parameters $A_{\alpha_i}, B_{\alpha_i}, C_{\alpha_i}, D_{\alpha_i}$ for both α_1 and α_2 cases. For all time t we have

$$\left.\begin{aligned} \frac{A_{\alpha_1}}{D_{\alpha_1}} &= 0.5430755797\cdots, & \frac{A_{\alpha_2}}{D_{\alpha_2}} &= -0.2189232333\cdots, \\ \frac{B_{\alpha_1}}{D_{\alpha_1}} &= 0.2030285360\cdots, & \frac{B_{\alpha_2}}{D_{\alpha_2}} &= 3.042085395\cdots, \\ \frac{C_{\alpha_1}}{D_{\alpha_1}} &= -0.3738495065\cdots, & \frac{C_{\alpha_2}}{D_{\alpha_2}} &= 13.89567161\cdots, \end{aligned}\right\} \tag{A 13}$$

where $D_{\alpha_1}(t)$ and $D_{\alpha_2}(t)$ are parameters to be determined from the outer solution of the problem.

The asymptotic expansion (A 11) shows that the viscous flow near the corner is composed of two dominant modes related to the functions $f_{\alpha_1}(\theta)$ and $f_{\alpha_2}(\theta)$. To demonstrate the nature of each mode, we present in figure 22 streamline patterns according to (A 11) where $D_{\alpha_1} = 1$ and $D_{\alpha_2} = 0$ (figure 22*a*) and $D_{\alpha_1} = 0$ and $D_{\alpha_2} = 1$ (figure 22*b*). It can be seen that the mode associated with the power $\alpha_1 = 1.5444837368\cdots$ describes a smooth turning of the flow around the corner without any separation, whereas the mode associated with the power $\alpha_2 = 1.9085291895\cdots$ describes a flow separation with a straight separation line originating from the corner and oriented at 135° from both walls creating the corner. In a viscous flow around a corner both effects may take place and the local flow is determined from the values of the parameters $D_{\alpha_1}(t)$ and $D_{\alpha_2}(t)$. When $|D_{\alpha_1}(t)| \gg |D_{\alpha_2}(t)|$, which is typical of relatively low-Re flows ($Re < 1$), the smooth turning of flow dominates the corner region. However, when $|D_{\alpha_2}(t)|$ is of the order of $|D_{\alpha_1}(t)|$, which is typical of high-Re flows ($Re > 20$), the mode of separation combines in a nonlinear way with the smooth flow turning mode to create a complicated local flow region very close to the corner.

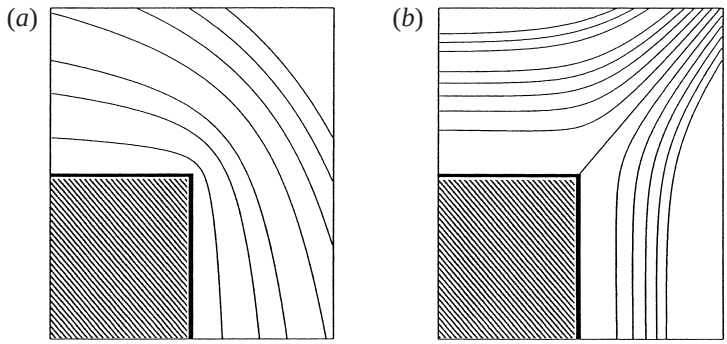

FIGURE 22. Streamline patterns according to (A 11) for (*a*) smooth flow mode, (*b*) separated flow mode.

Using the above solution (A 11) for ψ we can continue the asymptotic analysis and show that the third-order term in the expansion (A 5) must be $O(D_{\alpha_1}^2(t)Re\, r^{2\alpha_1})$. In summary, we may conclude that as r tends to zero the local flow around the corner is described by

$$\psi(r,\theta,t) = \psi_0 + D_{\alpha_1}(t)r^{\alpha_1}f_{\alpha_1} + D_{\alpha_2}(t)r^{\alpha_2}f_{\alpha_2} + O(D_{\alpha_1}^2(t)Re\, r^{2\alpha_1}). \tag{A 14}$$

This result shows that the asymptotic expansion (A 14) for $\psi(r,\theta,t)$ near the corner is valid when the distance r from the corner satisfies

$$0 \leqslant r \ll \frac{1}{Re^{1/\alpha_1}}. \tag{A 15}$$

Consequently, the local asymptotic solution describing the flow around the corner is given by (A 14) with

$$\Omega(r,\theta,t) = -D_{\alpha_1}(t)r^{\alpha_1-2}[\alpha_1^2 f_{\alpha_1}(\theta) + f_{\alpha_1}^{(II)}(\theta)] - D_{\alpha_2}(t)r^{\alpha_2-2}[\alpha_2^2 f_{\alpha_2}(\theta) + f_{\alpha_2}^{(II)}(\theta)] + O(D_{\alpha_1}^2(t)Re\, r^{2\alpha_1-2}), \tag{A 16}$$

$$p(r,\theta,t) = p_0 + D_{\alpha_1}(t)\frac{1/Re}{(\alpha_1-2)}r^{\alpha_1-2}(\alpha_1^2 f_{\alpha_1}(\theta) + f_{\alpha_1}^{(II)}(\theta))^{(I)} + D_{\alpha_2}(t)\frac{1/Re}{(\alpha_2-2)}r^{\alpha_2-2}(\alpha_2^2 f_{\alpha_2}(\theta) + f_{\alpha_2}^{(II)}(\theta))^{(I)} + O(D_{\alpha_1}^2(t)r^{2\alpha_1-2}). \tag{A 17}$$

It can be seen that the velocity components tend to zero as the corner is approached and that the vorticity, the pressure, and the other stress components are all singular at the corner.

REFERENCES

ALLEBORN, N. NANDAKUMAR, K., RASZILLIER, H. & DURST, F. 1997 Further contributions on the two-dimensional flow in a sudden expansion. *J. Fluid Mech.* **330**, 169–188.

BATCHELOR, G. K. 1967 *An Introduction to Fluid Dynamics*. Cambridge University Press.

BATTAGLIA, F., TAVENER, S. J., KULKARNI, A. K. & MERKLE, C. L. 1997 Bifurcation of low Reynolds number flows in symmetric channels. *AIAA J.* **35**, 99–105.

CHERDRON, W., DURST, F. & WHITELAW, J. H. 1978 Asymmetric flows and instabilities in symmetric ducts with a sudden expansion. *J. Fluid Mech.* **84**, 13–31.

CHESSHIRE, G. & HENSHAW, W. D. 1990 Composite overlapping meshes for the solution of partial differential equations. *J. Comput. Phys.* **90**, 1–60.

Cole, J. D. & Schwendeman, D. W. 1990 Hodograph design of shock-free transonic slender bodies. *Proc. 3rd Intl Conf. Hyperbolic Problems, Uppsala, June 11–15* (ed. B. Engquist & B. Gustafsson), Vol. 1, pp. 255–269.

Drikakis, D. 1997 Bifurcation phenomena in incompressible sudden expansion flows. *Phys. Fluids* **9**, 76–87.

Durst, F., Melling, A. & Whitelaw, J. H. 1974 Low Reynolds number flow over a plane symmetrical sudden expansion. *J. Fluid Mech.* **64**, 111–128.

Durst, F., Pereira, J. C. F. & Tropea, C. 1993 The plane symmetric sudden expansion flow at low Reynolds numbers. *J. Fluid Mech.* **248**, 567–581.

Fearn, R. M., Mullin, T. & Cliffe, K. A. 1990 Nonlinear flow phenomena in a symmetric sudden expansion. *J. Fluid Mech.* **211**, 595–608.

Hawa, T. & Rusak, Z. 2000 Viscous flow in a slightly asymmetric channel with a sudden expansion. *Phys. Fluids* **12**, 2257–2267.

Hoffmann, K. A. & Chiang, S. T. 1998 *Computational Fluid Dynamics for Engineers*, vol. 1. EES.

Moffatt, H. K. 1964 Viscous and resistive eddies near a sharp corner. *J. Fluid Mech.* **18**, 1–18.

Rusak, Z. & Hawa, T. 1999 A weakly nonlinear analysis of the dynamics of a viscous flow in a symmetric channel with a sudden expansion. *Phys. Fluids* **11**, 3629–3636.

Shapira, M., Degani, D. & Weihs, D. 1990 Stability and existence of multiple solutions for viscous flow in suddenly enlarged channels. *Computers Fluids* **18**, 239–258.

Sobey, I. J. 1985 Observation of waves during oscillatory channel flow. *J. Fluid Mech.* **151**, 395–426.

Sobey, I. J. & Drazin, P. G. 1986 Bifurcations of two-dimensional channel flows. *J. Fluid Mech.* **171**, 263–287.

Soong, C. Y., Tzeng, P. Y. & Hsieh, C. D. 1998 Numerical investigation of flow structure and bifurcation phenomena of confined plane twin-jet flows. *Phys. Fluids* **10**, 2910–2921.